Nonequilibrium relaxation method

2007 J. Phys. A: Math. Theor. 40 R149

(http://iopscience.iop.org/1751-8121/40/31/R01)

J. Phys. A: Math. Theor. **40** (2007) R149–R203 doi:10.1088/1751-8113/40/31/R01

TOPICAL REVIEW

Nonequilibrium relaxation method

Yukiyasu Ozeki[1] **and Nobuyasu Ito**[2]

[1] Department of Applied Physics and Chemistry, The University of Electro-Communications, Chofugaoka 1-5-1, Chofu city, Tokyo 182-8585, Japan
[2] Department of Applied Physics, Graduate School of Engineering, The University of Tokyo, Bunkyo-ku, Hongo, Tokyo 113-8656, Japan

Received 28 February 2007, in final form 7 June 2007
Published 19 July 2007
Online at stacks.iop.org/JPhysA/40/R149

Abstract
The nonequilibrium relaxation (NER) method is a numerical technique to analyse equilibrium phase transitions. One can estimate the transition point and critical exponents calculating relaxations of order parameter and fluctuations in NER processes from nonequilibrium initial states to the equilibrium ones. It is applied to the second-order transition as well as the first-order one; the precise estimation of transition temperature for the latter case is achieved with the mixed phase initialization technique. Since the equilibration is not necessary in the simulation, one can analyse systems with large sizes which can be recognized as in the thermodynamic limit up to the observation time. This leads to the analysis being more efficient for slowly relaxing systems with frustrations and randomness. It can be extended to the Kosterlitz–Thouless transition and the spin glass transition cases by the use of the finite-time scaling analysis. It is also extended to quantum systems.

PACS number: 64.60.−i

Contents

1. Introduction

Questions such as 'What kind of phase appears with this interaction?' or 'How do we apply interactions to realize this phase?' arise frequently in material sciences and technologies. The analysis of phases and transitions based on a microscopic model is an important technique in statistical physics. Precise phase diagrams and values of critical exponents have not only physical significance, but also applicability to many fields such as engineering, sociology, economics, environmentology, and so on. For example, the phase transition between water and vapour is one of the main problems in power-engineering, and the transition between vapour, water and ice strongly influences the global environment. To answer such questions, the statistical physics provides a standard prescription based on the free energy function. One estimates the free energy as a function of thermodynamic parameters such as the temperature, the external field and so on, differentiates it by one or some of these parameters to obtain thermodynamic quantities, and then analyses them. Although this procedure is general and well established, and has been working successfully to predict some rather simple systems such the ideal gas and special models [1], it is exceptional in real problems where a direct application of the equilibrium statistical mechanics is somehow pie in the sky. Calculations of rigourous free energies are hard in most cases. One of the main purposes in statistical physics is to overcome this difficulty. In analytic methods such as the mean field theory, the renormalization group (RG) method and the series expansion, some approximations, which sometimes mislead the result, are necessary, and one needs experience as well as a great physical insight in the problem.

Since the middle of the last century, numerical analyses based on the computational physics have been studied actively [2–4] along with the computer development [5]. The equilibrium Monte Carlo simulation (EMCS), the exact diagonalization, the numerical transfer matrix method and so on provide numerically reliable estimations of physical quantities for specific values of parameters on a finite size system. Together with the finite size scaling analysis [6], one can investigate thermodynamic and critical properties of the system. In most numerical methods, available systems are, however, restricted because of limitations of the computational time and the storage size, which sometimes restrict the size of the system and/or

the dimensionality—required linear sizes are often unreachable in higher dimensions. The most popular method is the EMCS, since the above restriction is not so strong [7] compared with exact enumeration methods. And it is general and applicable to a wide variety of systems. While the EMCS is powerful in many cases, it suffers difficulties in some systems such as frustrated systems, random systems, Kosterlitz–Thouless (KT) transition systems, and weak first-order transition systems, which have been investigated much recently. In these systems, slow relaxation appears near the transition point, and the equilibration and/or the statistical averaging take much computational time. Studies and development on the EMCS in last decades, such as the cluster algorithm [8–10], the multi-canonical method [11–13] and so on, have devoted to overcome these difficulties. While they are successful to improve the efficiency of calculations, the algorithm and the computational code become more complicated and the applicability becomes more restricted [14]. Thus, it is highly desirable to develop a numerical method with simple algorithms and wide applicabilities.

In the last decade, the nonequilibrium relaxation (NER) method has been developed to answer the above questions partly and satisfies these requests for wide variety of systems. In this method, equilibrium properties of a statistical model can be analysed through a dynamical behaviour from a nonequilibrium initial state to the equilibrium one. This NER process is nothing but the process discarded as the equilibration in the EMCS. Since the dawn of the EMCS, the NER process has appeared in each simulation, while it had not attracted much attentions. In early days when the computational power was not so high, the system size and the number of samples in a simulation were not enough to see relevant behaviour to understand the thermodynamic properties. People have considered that it was not so useful to study thermal properties. With the progress of computational environment, the available system has been increased and the importance of NER process has been easier to be recognized in simulations. The study of NER process is based on the dynamic finite-size scaling hypothesis [15–17], in which the observation time is recognized as one of the relevant scaling fields. This theory was followed by some NER studies [18–25]. It was observed that shorter scale structures relax quickly, which confirms that the equilibrium properties can be investigated in the NER process [25]. In early stage, the NER process was applied to investigate the dynamic critical behaviour [26–32]. The cluster dynamics was also studied from the NER of energy [33]. Since 1990s, it has been applied to quantitative analyses, and we have called it 'the NER method'. It can be applied to a wide variety of phases and transitions in various statistical models.

The computer simulation is now indispensable tool of theoretical physics. In the field of statistical physics, its importance has been also increasing, because it can treat various systems and phenomena which are difficult to be studied by analytic methods. The standard EMCS strategy is described as follows. First, realize the equilibrium ensemble of a finite system, then estimate the thermal averages, and finally extrapolate them to an infinite-size limit or analyse them using the scaling theory. The NER method provides a new strategy of numerical simulations. Instead of the EMCS analysis, we examine how the system relaxes to the equilibrium state in the NER process, and extract the nature of the equilibrium state. It is useful not only for numerical study but also for analytic study [32]. One can estimate the transition temperature as well as various critical exponents [34–37]. The NER simulation has some excellent features as a numerical analysis. First, the system-size dependence of the NER function at a fixed time t is exponentially small even at the transition point [28]. This feature is understood from the fact that the correlation length $\xi(t)$ is finite at finite times. So the value in the thermodynamic limit is easily estimated. Second, the equilibration steps are not necessary in the analysis. A simulation is made only up to the steps when the asymptotic behaviour can be identified from the faster modes. Therefore, the NER method is useful to study systems in which strong fluctuations appear or sufficient sizes cannot be prepared on

account of large equilibration time. It is appropriate much to study frustrated and/or random systems.

In the present review, we review the NER method and its applications. In section 2, the basic idea of the NER analysis is described. We introduce a method to estimate the transition temperature for second-order transition systems together with that for a dynamical exponent. In section 3, the static exponents, α, β, ν as well as the dynamical one, z, are estimated individually by the analysis of the NER of fluctuations. For the case of first-order transitions, the hysteresis phenomenon in the NER process is demonstrated in section 4, which reveals the confirmation of the first-order transition. The mixed phase initialization is also introduced there, which provides a precise estimation of the transition point. The advantage of the NER method to the EMCS is discussed in section 5. Some successful applications are presented. In section 6, a scaling analysis for KT transitions is introduced to estimate the transition temperature precisely. Since the correlation length diverges whole in the KT phase, it is somehow difficult to estimate it numerically. The present method with the scaling analysis is simple and reliable providing the applicability to various problems. The estimation for critical exponents just at the KT transition point is also introduced. We introduce the NER analysis for spin glass (SG) transitions in section 7. Two kinds of dynamical quantities are proposed to estimate the transition temperature and exponents by the use of dynamical scaling hypothesis. In section 8, the method is extended to quantum cases. The last section is devoted to some remarks.

2. NER analysis of order parameter

In an NER process from a definite initial state, every thermodynamic quantity shows a temporal relaxation. We call such a time-dependent quantity, the NER function. Except at the transition point, each NER function decays exponentially to the thermal equilibrium value and it decays algebraically at the transition point—the critical point. (Here, we assume a continuous phase transition. The first-order transition case will be discussed later.) The phase at a specific set of thermodynamic parameters is identified by observing the behaviour of NER functions. The most useful NER function is the relaxation of order parameter from a complete ordered initial state, i.e. the magnetization from the all-aligned state in the ferromagnetic (FM) case.

2.1. NER of order parameter

The first step of the NER analysis is based on the relaxation of order parameter

$$m(t) \equiv \langle \hat{m} \rangle_t, \tag{2.1}$$

which gives the estimations of the transition temperature and a dynamical exponent. Here, $\hat{m}$ represents the operator of order parameter and $\langle \cdots \rangle_t$ denotes a dynamical average at time t. To see the standard procedure of the NER analysis, let us consider the NER process from an all-aligned state in a simple second-order FM transition system. At the initial state ($t = 0$), the magnetization is saturated as $m(0) = 1$. As mentioned above, we expect that $m(t)$ decays exponentially to zero in the paramagnetic (PM) phase, and so does algebraically at the transition point. In the FM phase, it decays to the spontaneous value $m_{\rm eq}$ exponentially. The asymptotic behaviour of magnetization $m(t)$ is summarized as

$$m(t) \sim \begin{cases} \exp(-t/\tau) & (T > T_{\rm c}) \\ t^{-\lambda_m} & (T = T_{\rm c}) \\ m_{\rm eq} & (T < T_{\rm c}), \end{cases} \tag{2.2}$$

where τ is the relaxation time and λ_m is the dynamical exponent which characterizes the power-law decay of the magnetization at the critical point. Precisely speaking, the exponential decay terms in equation (2.2) may include a faster decay factor such as an algebraic one t^{-x} or may be substituted by a term faster than any power law. In any cases, we can distinguish three regimes, $T > T_c$, $T = T_c$, and $T < T_c$, from the asymptotic behaviour of $m(t)$. Note that the crossover time after which the above asymptotic behaviour can be observed depends on various factors in the system, and cannot be discussed here in general.

At any temperature, the initial nonequilibrium state contains various relaxation modes. At the beginning, the NER function shows an initial relaxation, and then, approaches to the asymptotic behaviour. The initial relaxation exhibits the process in which the weights of faster relaxation modes are reduced one after another. Practically, there is a problem how we distinguish the initial relaxation and the asymptotic behaviour from numerical data. Although the NER function behaves non-monotonically at the beginning of the relaxation, this problem is not serious in the determination of the critical point. If one sees the NER function of several temperatures around the critical point, all curves behave coherently in the initial relaxation. The structure of faster modes seems to be qualitatively similar even around the critical point. Thus, even if the NER function shows a non-monotonic behaviour, one can recognize it as the initial relaxation. On the other hand, in the asymptotic regime, the structure of relaxation modes changes drastically at the critical point. This provides the difference in equation (2.2) or the upward-turn and downward-turn behaviour in the local exponent (see section 2.3). Therefore, if one sees a qualitative change in the behaviour of the NER function (or the local exponent) at a particular temperature, one can conclude it as the critical temperature.

Note that the above-mentioned behaviour of the NER magnetization is valid in the thermodynamic limit, while we can use numerical data for finite systems. Practically, we analyse data calculated by Monte Carlo simulations on finite lattices, in which one cannot define the spontaneous magnetization in equilibrium because of the spin-reversal symmetry. On the other hand, in the NER from the all-aligned state, the magnetization remains finite after statistical averaging in some time scale. To understand it, let us consider the dynamical correlation length $\xi(t)$ in which spins correlate with each other actively at time t. It can be defined from a dynamical correlation function [20] as

$$G(r, t) \sim \exp[-r/\xi(t)]. \tag{2.3}$$

In general, $G(r, t)$ is defined through a dynamical quantity $\hat{Q}$ as

$$G(r, t) \equiv \langle \hat{Q}_0 \hat{Q}_r \rangle_t - \langle \hat{Q}_0 \rangle_t \langle \hat{Q}_r \rangle_t, \tag{2.4}$$

where $\hat{Q}_0$ and $\hat{Q}_r$ are operators of the quantity at a distance of r. Let us denote the linear size of the system by L. The dynamical correlation length is vanishing at the initial all-aligned state, $\xi(0) = 0$, and evolves in time up to the equilibrium value ξ_{eq}. Using $\xi(t)$, we derive the correlating time (or the relaxation time) $\tau(r)$ after which the spins in a distance of r begin to correlate actively with each other. The function $\tau(r)$ is defined as the solution of

$$\xi[\tau(r)] = r. \tag{2.5}$$

Roughly speaking, spins in a range longer than $\xi(t)$ behave independently. Thus, in a time interval with $L \gg \xi(t)$ or equivalently $t \ll \tau(L)$, almost all spins are independent of the boundary, and the observed NER can be regarded as in the thermodynamic limit. The magnetization remains finite after statistical averaging in the NER from the all-aligned state when $L \gg \xi(t)$, since the spin-reversal symmetry has already been broken in the initial state and the effect keeps up to the time $t = \tau(L)$.

In practice, the NER of (per-site) order parameter $m(t)$ is calculated by a Monte Carlo simulation with any of local-spin-updating algorithms. The statistical averaging is performed

by the independent sampling of time evolution; one repeats simulations from the initial state by changing random numbers in Monte Carlo dynamics, and averages the observed quantities over the simulations. One does not need to anxious about 'so-called' systematic errors due to dynamical correlations, which often appears in standard EMCS. In EMCS, the importance sampling is used for statistical averaging, in which equilibrium ensemble is generated by a time sequence in a particular dynamics with detailed balance. Thus, the sampling is not completely independent. This sometimes causes a serious error in the data and misleads the result.

In an NER simulation with a standard Monte Carlo algorithm, the total calculation time is proportional to the total number of updated spins N_{updated}. It can be expressed by the number of spins N, the number of samples for statistical averaging N_{av} and the maximum observation steps $t_{\max}$ as

$$N_{\text{updated}} = N \times N_{\text{av}} \times t_{\max}. \tag{2.6}$$

If $t_{\max}$ is less than the correlating time $\tau(L)$ defined in equation (2.5), one may consider the simulated system as in the thermodynamic limit, and the statistical error for one sample is proportional to $1/\sqrt{N}$ and that for averaged $m(t)$ at each step is given by

$$|\Delta m(t)| \propto \frac{1}{\sqrt{N N_{\text{av}}}}. \tag{2.7}$$

Let us consider the case with fixed N_{updated}, which means that the total computational time is restricted. The maximum observation time $t_{\max}$ should be fixed as is sufficient to understand thermodynamics properties. Then, $N \times N_{\text{av}}$ is a constant and the resulting statistical error is independent of how one chooses the system size N. Larger sizes are preferable for the analysis, since one can observe the thermodynamic behaviour for longer time scale. Therefore, one may choose the system size as large as possible; usually it is restricted by the storage size.

Here, we restrict our attention to the second-order transition case in which the order parameter is defined definitely, and the initial complete ordered state is known. Of course, one may consider other cases such as the complete ordered state is unknown, the order parameter is unknown, the long-range order is absent, the first-order transition. In latter cases, we need to modify something in the above procedure.

2.2. Dynamical scaling

The dynamical exponent λ_m defined in equation (2.2) is related to conventional exponents including the dynamical exponent z. In standard second-order transition systems approaching to the critical point, the correlation length ξ_{eq} and the relaxation time τ_{eq} diverge. The amount of ξ_{eq} indicates the length scale of strongly correlated regime in equilibrium, and τ_{eq} is the time scale of the correlation falling into oblivion. The exponent z is defined as

$$\tau_{\text{eq}} \sim \xi_{\text{eq}}^{z}. \tag{2.8}$$

In a normal diffusion process where only a microscopic change occurs in a unit time, we expect $z = 2$. In a Monte Carlo dynamics with a local-spin-updating algorithm, the time evolution is like microscopic and diffusive. Then, we expect $z \sim 2$, while it is deviated because of the critical fluctuation.

In the previous subsection, we defined the dynamical correlation length $\xi(t)$ in equation (2.3), in which spins correlate with each other actively at time t, and the correlating time $\tau(r)$ in equation (2.5), after which the spins in a distance of r begin to correlate actively with each other. We have mentioned that the NER behaviour is not affected by the finiteness of the lattice in a time interval with $t \ll \tau(L)$. In other words, the NER behaviour shows

a remarkable finite size crossover at around $t = \tau(L)$. According to the finite size scaling hypothesis together with the dynamical crossover behaviour, one expects the scaling function of the NER of magnetization as [15–17]

$$m(T, t, L) = L^{-\beta/\nu}\bar{m}[L/\xi_{\rm eq}, t/\tau(L)]. \tag{2.9}$$

At around the critical point, $\xi(t)$ and $\tau(L)$ approach the equilibrium correlation length $\xi_{\rm eq}$ for large t and the relaxation time $\tau_{\rm eq}$ for large L, respectively. From equations (2.5) and (2.8), the asymptotic power of $\tau(L)$ is expected as

$$\tau(L) \sim L^{z}. \tag{2.10}$$

Thus, we obtain the homogeneous form

$$m(T, t, L) = L^{-\beta/\nu}\bar{m}(\varepsilon L^{1/\nu}, tL^{-z}), \tag{2.11}$$

where ε is the reduced temperature

$$\varepsilon = \left|\frac{T - T_{\rm c}}{T_{\rm c}}\right|. \tag{2.12}$$

Setting $tL^{-z} = c$ and $T = T_{\rm c}$, we obtain the relation [15, 16]

$$\lambda_m = \frac{\beta}{z\nu}. \tag{2.13}$$

2.3. Local exponent

To see the asymptotic power-law decay of the NER function $m(t)$ clearly, we usually analyse its logarithmic derivative,

$$\lambda_m(t) \equiv -\frac{{\rm d}\log m(t)}{{\rm d}\log t}, \tag{2.14}$$

which is practically more convenient. We call it the local exponent (of $m(t)$). This name was called the effective exponent at the dawn of NER study [26, 28, 29]. It is noted that the dynamical function $\lambda_m(t)$ should be distinguished from the exponent λ_m which is a constant in time. We will use the same conventions for other exponents.

Let us examine three typical behaviour in equation (2.2). With the local exponent $\lambda_m(t)$, the asymptotic behaviour of $m(t)$ is identified precisely. For the case of exponential decay to zero,

$$m(t) = A\exp(-t/\tau_{\rm eq}), \tag{2.15}$$

the local exponent is given by

$$\lambda_m(t) = -\frac{{\rm d}\log m(t)}{{\rm d}\log t} = \frac{t}{\tau_{\rm eq}}. \tag{2.16}$$

It approaches infinity when $t \to \infty$ even if the exponential term includes an algebraic factor or is substituted by a term faster than any power law. For the case of exponential decay to a positive spontaneous value

$$m(t) = A\exp(-t/\tau_{\rm eq}) + B, \tag{2.17}$$

the local exponent behaves as

$$\lambda_m(t) = \frac{t}{\tau}\frac{A}{A + B\exp(t/\tau_{\rm eq})}. \tag{2.18}$$

It is vanishing when $t \to \infty$ even if the exponential term is modified. For the last case, the power-law decay to zero

$$m(t) = At^{-\lambda_m}(1 + B/t^{\omega}), \tag{2.19}$$

the local exponent obeys

$$\lambda_m(t) = \lambda_m + \frac{\omega B}{t^{\omega} + B}. \tag{2.20}$$

It converges to a nonzero definite value λ_m when t goes to infinity. Here, the correction term (B/t^{ω}) is included for general considerations, which relates to the corrections to scaling for equation (2.11) originated in a irrelevant scaling field. Consequently, we obtain the asymptotic behaviour

$$\lambda_m(t) \to \begin{cases} \infty & (T > T_c) \\ \lambda_m & (T = T_c) \\ 0 & (T < T_c). \end{cases} \tag{2.21}$$

From the numerically calculated NER function $m(t)$, the local exponent $\lambda_m(t)$ is estimated by several ways. One is to calculate the quantity [26, 28, 29],

$$\frac{t}{\Delta t}\left(\frac{m(t - \Delta t)}{m(t)} - 1\right). \tag{2.22}$$

It is useful not only in numerical study, but also in analytic study [32]. It is easily evaluated, while the statistical fluctuation is large. Therefore, we need a large number of samples for statistical averaging. Another one, more practical way, is to use a numerical derivative of the $\log t - \log m(t)$ curve; one may fit a line to data points of $(\log t, \log m(t))$ in the time interval $[t, t + \Delta t]$ with appropriately chosen Δt, which may depend on t.

2.4. Estimation of transition temperature

To estimate the transition temperature, the NER method provides a simple procedure for standard second-order transition cases. In principle, equation (2.2) or equivalently equation (2.21) which is more practical are used to identify the phase at each temperature.

As an example, let us see the NER analysis for the FM Ising model in three dimensions [37–40]. The Hamiltonian is given by

$$\mathcal{H} = -J \sum_{\langle ij \rangle} S_i S_j \qquad (S_i = \pm 1), \tag{2.23}$$

with the summation taken over the bonds on the simple cubic lattice. First, we show a typical behaviour of $m(t)$ and $\lambda_m(t)$. A Monte Carlo simulation is performed by the Metropolis dynamics with two-sublattice updating algorithm. The NER of magnetization from an all-aligned state is estimated at several temperatures around expected transition temperature. In figure 1, typical behaviour of $m(t)$ are plotted with the double-log scale for $K = 0.2212$, $K = 0.221\,6545 \simeq K_c$ and $K = 0.2220$, where we use the inverse temperature $K \equiv J/k_B T$. Calculations are performed on the $101 \times 101 \times 100$ cubic lattice up to 100 MCS (Monte Carlo steps). At each temperature, 320 independent samples (time sequences) are used for statistical averaging. By careful observation, one can find the difference of asymptotic behaviour; one is bending up slightly at $K = 0.2220$ indicating the asymptotic saturation in the FM phase and one is bending down at $K = 0.2212$ indicating the exponential decay in the PM phase.

While this observation could be somehow subjective in the plot of $m(t)$, it can be clarified in the plot of local exponent $\lambda_m(t)$ versus $1/t$ in figure 2. To identify the phase from the

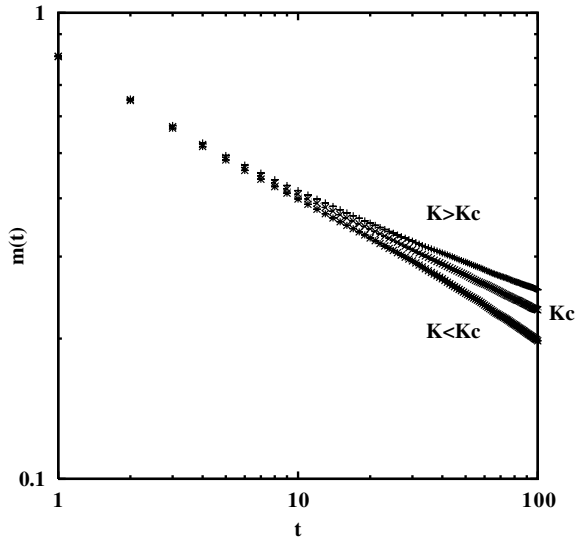

Figure 1. Typical behaviour of the NER of order parameter for the 3D FM Ising model is plotted for $K = 0.2212 < K_c$, $K = 0.221\,6545 \simeq K_c$ and $K = 0.2220 > K_c$.

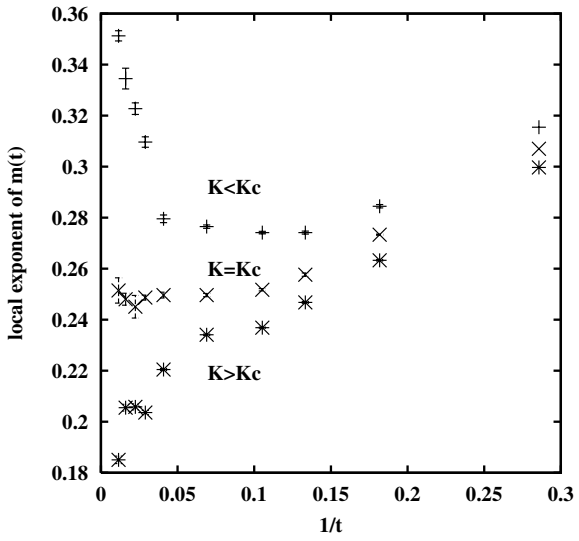

Figure 2. Local exponent $\lambda_m(t)$ for the 3D FM Ising model corresponding to figure 1 is plotted.

asymptotic behaviour of the local exponent in the limit of $t \to \infty$, its plot versus $1/t$ (or $1/t^{\omega}$ with appropriately selected ω) is useful. As shown in equation (2.21), at the critical point where $m(t)$ decays to zero algebraically, the local exponent $\lambda_m(t)$ approaches a nonzero definite value in the limit of $1/t = 0$. When $m(t)$ decays exponentially to zero, $\lambda_m(t)$ shows a strong crossover from finite values to diverging. The curve turns up around the crossover time and grows in the limit of $1/t = 0$. Observing behaviour of $m(t)$ at several temperatures

around $T = T_c$, one can estimate the upper bound of T_c as the minimum temperature showing this behaviour. When $m(t)$ decays exponentially to a positive value, $\lambda_m(t)$ shows a cross over from finite values to vanishing. The curve turns down to zero in the limit of $1/t = 0$. One can estimate the lower bound of T_c as the maximum temperature showing this behaviour. Then, the true transition temperature is concluded to lie between these bounds. The estimation is given by the centre of the bounds and the error bar is put between them. It is clearly seen in figure 2 that the curve turns down at $K = 0.2212$ for $1/t \to 0$ and turns down at $K = 0.2220$, which is consistent with the above direct observation for $m(t)$. This provides the estimation of the transition temperature $K_c = 0.2216(4)$.

The error bar in the present method is highly reliable in the sense that it is hard to find the true transition point out of this range if the observed behaviour is the asymptotic one. As mentioned above, it is easy to check that the observed behaviour is identical with that in the thermodynamic limit. If the observed behaviour is really the asymptotic one, such an estimation is preferable as compared with the result obtained by the scaling analysis in the EMCS, where one put the error bar due to some criterion—smoothness of fitting, smallest statistical deviation, or something—which is not always valid if the sample-to-sample correlation in the importance sampling or the finite size effect are remarkable. Of course, the confirmation of the asymptotic relaxation in the NER analysis is not always easy for some complicated systems, one need to check the result by other methods such as the EMCS.

To get a higher precision for the estimation of transition temperature, one needs to perform simulations for higher resolution of observed temperatures, which gives data for temperatures closer to the transition point. For temperatures close to the transition point, the crossover time after which asymptotic behaviour can be distinguished becomes long—it is of the order of $\varepsilon^{-z\nu}$. Thus, longer observations are necessary, which reveal simulations with more samples to keep the same order of statistical error. We have performed a simulation on a larger lattice ($6648 \times 6648 \times 6656$) up to a longer time ($10^5$ MCS) [40]. The behaviour of $\lambda_m(t)$ at six typical temperatures which are closer to the above case is given in figure 3. Note that the time interval plotted there becomes much longer. It turns up in the limit of $1/t = 0$ at $K = 0.221\,6542$ providing the PM behaviour, and it turns down at $K = 0.221\,6552$ providing the FM behaviour. Consequently, the transition point lies in $0.221\,6542 < K_c < 0.221\,6552$ and the estimation

$$K_c = 0.221\,6547(5) \tag{2.24}$$

is obtained. This result was compared with other estimations: high-temperature expansion [41], scaling [42], spontaneous magnetization [43] and Monte Carlo renormalization group results [44–48]. It was found that the NER method has competitive accuracy while it is much simpler than other methods. Since the error bars estimated in the NER method are not statistical, but are obtained from upper and lower bounds of the transition point in the thermodynamic limit, the result is much reliable.

2.5. Finite-size correction

In the previous section, the NER of magnetization for the thermodynamic limit is discussed. In the scaling region, the physical quantity usually depends on some power of size. Therefore, an appropriate extrapolation procedure or scaling analysis in terms of the system size is necessary in the EMCS. On the other hand, it is simple and straightforward in the NER analysis. It is often very easy to estimate the values of NER functions in the thermodynamic limit numerically even at the transition point.

Let us denote an NER function in a system with the size L as $f(t, L)$. Since it decays from a given nonequilibrium state, it does practically not depend on L until the dynamical

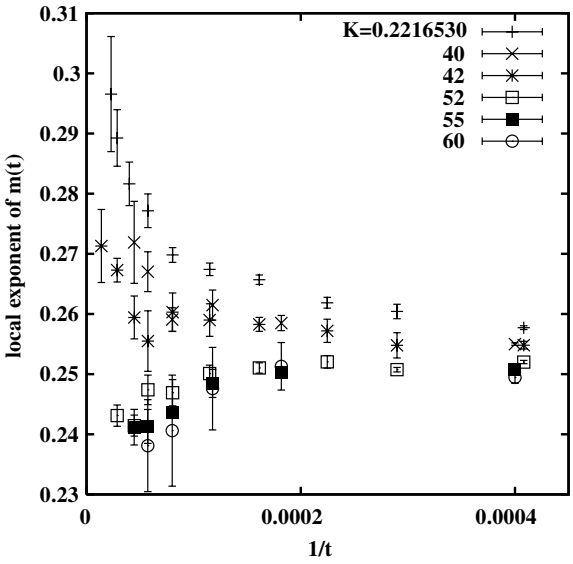

Figure 3. Local exponent $\lambda_m(t)$ for the 3D FM Ising model is plotted [40] to improve the estimation of the transition temperature obtained from figure 2.

correlation length $\xi(t)$ grows up to the order of L namely $t \sim \tau(L)$. When the system size is selected to be much larger than the equilibrium correlation length $\xi_{\rm eq}$, the finite-size correction is negligible at any time. Even when $\xi_{\rm eq} = +\infty$, it takes time of the order of L^z until $\xi(t) \sim L$. In other word, the L-dependence of $f(t, L)$ is exponentially weak at any fixed t:

$$f(t, L) \sim f(t, \infty) + A\,{\rm e}^{-\kappa L}. \tag{2.25}$$

This behaviour is easily confirmed by Monte Carlo simulation [28]. One example is given in figure 4, which shows the finite-size correction in the NER of magnetization $m(t, L)$ for the FM Ising model in three dimensions. It is confirmed that the finite-size correction is exponentially small as is expressed by equation (2.25). In figure 4, it is found that the finite-size correction for the system with $L = 40$ is always less than $\sim 10^{-6}$ at $t = 200$ MCS. The value of $m(200, \infty)$ is about 0.2, therefore the size $L = 40$ is already sufficient to be regarded as the infinite system up to $t = 200$ MCS. If the lattice with $L = 100$ is used, we can observe the infinite-system behaviour up to $200 \times (100/40)^z \approx 1300$ MCS ($z = 2.06$).

2.6. Estimation of dynamical exponent

It is remarkable to show that the dynamical exponent z was estimated directly for the FM Ising model in two dimensions. In this model, the transition temperature ($T_{\rm c} = 2.269\cdots$) [3] and the static exponents ($\nu = 1, \beta = 1/8$) are known exactly, while the dynamical exponent has not yet been obtained. Many analytical and numerical studies to estimate its value have been presented. The historical review of its estimation in the case of local dynamics, which does not update spins globally, is given in figure 5 [29, 31, 32].

The Monte Carlo simulation was performed on the lattice of 1501×1500 up to 400 MCS by the Metropolis dynamics with two-sublattice updating algorithm [29]. This size is

[3] Hereafter, we measure the temperature in a unit of $J/k_{\rm B}$ without any notification whole in this article.

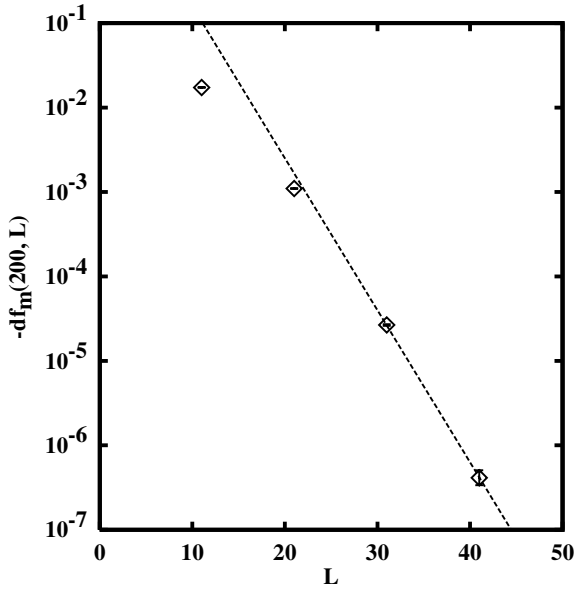

Figure 4. The finite-size correction, $df_m(t, L) = f_m(t, L) - f_m(t, \infty)$. Data for $t = 200$ MCS at the transition temperature in the 2D FM Ising model is plotted for several sizes [28]. The dashed line indicates $10 \times \mathrm{e}^{-0.414L}$.

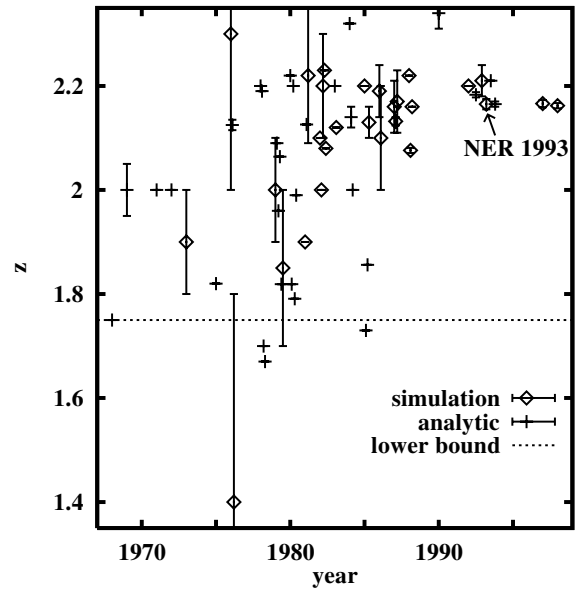

Figure 5. History for the estimation of the dynamical exponent in 2D FM Ising model [29]. Analytical and numerical estimations are plotted with + and ⋄, respectively. Horizontal dashed line at $z = 1.75$ shows the theoretical lower bound.

confirmed to be large enough to be regarded as the infinite system. The local exponent $\lambda_m(t)$ is estimated using equation (2.22) with $\Delta t = 1$. Since exact values of ν and β are known, the

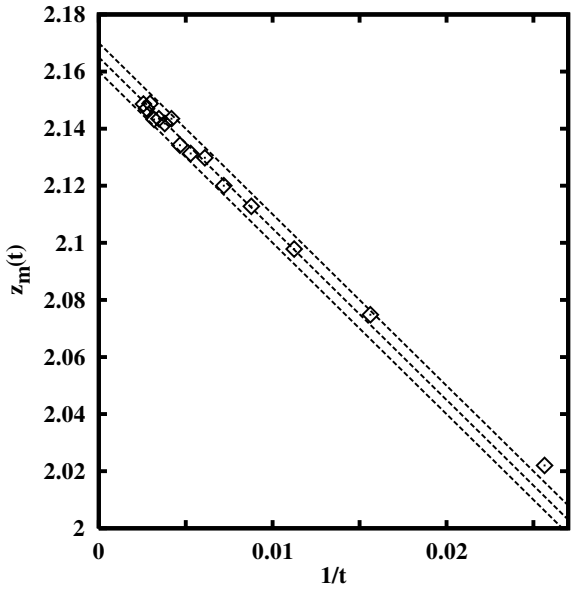

Figure 6. Local exponent $z(t) = \beta/\nu\lambda_m(t)$ for the 2D FM Ising model [29] is plotted as a function of $1/t$. Three lines are extrapolated to $z = 2.160$, 2.165 and 2.170.

local exponent defined by

$$z(t) = \frac{\beta}{\nu\lambda_m(t)} \tag{2.26}$$

can be plotted in figure 6. It is noted again as for $\lambda_m(t)$ that the dynamical function $z(t)$ should be distinguished from the exponent z which is a constant in time. The function $z(t)$ is expected to approach the value of z in the limit of $1/t = 0$ because of equation (2.13). It is observed in figure 6 that $z_(t)$ is extrapolated to $1/t = 0$ linearly. This means that the correction in equation (2.20) begins with a term of the order of $1/t$ and therefore $\omega \geqslant 1$ is expected. Three extrapolation lines are given in figure 6, and it is concluded as $z = 2.165(5)$, which is marked with 'NER 1993' in figure 5.

The NER method has been applied to study the dynamical universality. Wang and Hu [31] estimated the value of z to be 2.166(7), 2.164(7) and 2.170(10) for square, triangular and honeycomb lattices, respectively. These estimations are consistent with each other, and the dynamical universality is confirmed in this precision. The NER method is useful not only in numerical study but also in analytic one. Wang [32] studied the NER process of the 2D Ising model with the series expansion method, and obtained $z \approx 2.170$. Furthermore, it was shown that the combination of this series expansion and the Monte Carlo simulation provided $z = 2.169(3)$.

Furthermore, with the same NER analysis, the universality of the dynamical exponent z has been confirmed numerically for various class of models [49]. For the three-state Potts models on square, honeycomb and triangular lattices, the same value of $z = 2.20(1)$ is concluded, and for the Ising models on cubic, bcc and fcc lattices, the same value of $\lambda = 0.250(5)$ is concluded. It is confirmed that bond-alternating Ising models on square lattice are in the same dynamical universality class as the pure model, while randomly distributed models have been known to be in different universality.

3. NER analysis of fluctuations

3.1. NER functions of fluctuations

In the previous section, we show that one can estimate the transition temperature T_c and the dynamical exponent $\lambda_m = \beta/z\nu$ for standard second-order transition systems by analysing the NER of order parameter. If some exponents are known beforehand, the other exponent could be estimated as in the 2D FM Ising model in section 2.6. In contrast, in general case, we need to analyse further NER functions to estimate individual critical exponents [34–38, 50–52]. These functions are relating to quantities of fluctuations. So we call them 'NER of fluctuations'.

Let us consider, for example, the susceptibility χ_{eq} in equilibrium which diverges as $\varepsilon^{-\gamma}$ at the critical point. In the equilibrium statistical mechanics, it is expressed as

$$\chi_{eq} = \frac{N}{k_B T}\left(\langle \hat{m}^2 \rangle_{eq} - \langle \hat{m} \rangle_{eq}^2\right), \tag{3.1}$$

where $\langle \cdots \rangle_{eq}$ denotes the equilibrium averaging. For a standard relaxation process in which the system approaches the equilibrium state in time, if one defines the dynamical susceptibility

$$\chi(t) \equiv \frac{N}{k_B T}\left(\langle \hat{m}^2 \rangle_t - \langle \hat{m} \rangle_t^2\right), \tag{3.2}$$

it asymptotically approaches the equilibrium value χ_{eq} as $t \to \infty$. At the critical point, it is diverging asymptotically. Assuming the dynamical scaling for $\chi(t)$, one obtains a homogeneous scaling form

$$\chi(T, t, L) = L^{\gamma/\nu} \bar{\chi}(\varepsilon L^{1/\nu}, t L^{-z}), \tag{3.3}$$

as in equation (2.11) for $m(t)$. This provides the critical power-law divergence [20]

$$\chi(T_c, t, \infty) \sim t^{\gamma/z\nu}. \tag{3.4}$$

The same argument can be applied to the dynamical specific heat defined by

$$C(t) \equiv \frac{N}{k_B T^2}\left(\langle \hat{e}^2 \rangle_t - \langle \hat{e} \rangle_t^2\right), \tag{3.5}$$

where $\hat{e}$ denotes the energy per site at time t. It shows an asymptotic power-law divergence at the critical point as

$$C(t) \sim t^{\alpha/z\nu}. \tag{3.6}$$

Another useful quantity is the temperature derivative of the order parameter

$$\frac{\partial m_{eq}}{\partial T} = \frac{N}{k_B T^2}(\langle \hat{m}\hat{e} \rangle_{eq} - \langle \hat{m} \rangle_{eq} \langle \hat{e} \rangle_{eq}). \tag{3.7}$$

Since $\beta < 1$ in usual, it diverges as $\varepsilon^{\beta-1}$ at the critical point. If one defines the dynamical expression

$$m'(t) \equiv \frac{N}{k_B T^2}(\langle \hat{m}\hat{e} \rangle_t - \langle \hat{m} \rangle_t \langle \hat{e} \rangle_t), \tag{3.8}$$

it asymptotically approaches the equilibrium value $\frac{\partial m_{eq}}{\partial T}$ as $t \to \infty$ and is diverging at the critical point

$$m'(t) = t^{(1-\beta)/z\nu}. \tag{3.9}$$

We rearrange above quantities as dimensionless forms

$$f_{mm}(t) = N\left[\frac{\langle \hat{m}^2 \rangle_t}{\langle \hat{m} \rangle_t^2} - 1\right], \tag{3.10a}$$

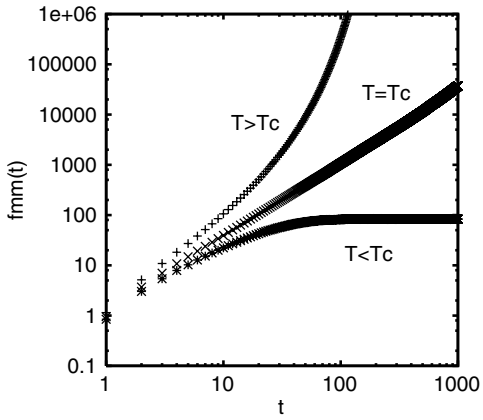

Figure 7. Typical behaviour of $f_{mm}(t)$ at $T = 4.4 < T_c$, $T = 4.451\,153 \simeq T_c$ and $T = 4.7 > T_c$ for the FM Ising model in 3D.

$$f_{me}(t) = N\left[\frac{\langle \hat{m}\hat{e}\rangle_t}{\langle \hat{m}\rangle_t \langle \hat{e}\rangle_t} - 1\right], \tag{3.10b}$$

$$f_{ee}(t) = N\left[\frac{\langle \hat{e}^2\rangle_t}{\langle \hat{e}\rangle_t^2} - 1\right], \tag{3.10c}$$

which are convenient for the estimation of individual exponents. To check the critical relaxations in equations (3.4), (3.6) and (3.9) and to see the standard behaviour of $f(t)$'s, we performed a Monte Carlo simulation for the FM Ising model in three dimensions. The NER of fluctuations is calculated on the $51 \times 51 \times 50$ simple-cubic lattice at $T = 4.4 < T_c$, $T = 4.451\,153 \simeq T_c$ and $T = 4.7 > T_c$. At each temperature, about 10^5 independent samples are used for statistical averaging. In figure 7, we plot $f_{mm}(t)$ as a function of t with a double-log scale. It is found that the function indicates a power-law divergence at $T = T_c$, which is consistent with equation (3.4). For $T < T_c$, it is saturated asymptotically indicating a finite susceptibility value. For $T > T_c$, while the susceptibility is finite, the NER function $f_{mm}(t)$ shows a strong divergence, which would be exponentially, because of the vanishing of m_{eq} in the denominator.

The behaviour of $f_{me}(t)$ is plotted in figure 8. At $T = T_c$, it shows a power-law divergence as in equation (3.9). For $T < T_c$, it is saturated asymptotically indicating a finite value of $\frac{\partial m_{eq}}{\partial T}$. For $T > T_c$, since both the denominator and the numerator in $f_{me}(t)$ are vanishing in equilibrium, the asymptotic value cannot be defined. Actually, it does not show a convergence in $t > 100$.

In figure 9, we plot $f_{ee}(t)$. It is easily seen that the function is saturated asymptotically for $T > T_c$ and $T < T_c$ indicating finite specific heat values. For $T = T_c$, while $f_{ee}(t)$ shows an increasing behaviour consistent with a power-law divergence as in equation (3.6) and the value is larger than those for out of criticality, it still does not show an asymptotic power law; it should be a straight line in the double-log plot for a single power-law divergence. A large corrections to scaling would be influenced.

Consequently, the NER functions of fluctuations in equations (3.10*a*)–(3.10*c*) are expected to show power-law divergence asymptotically at the critical point

$$f_{mm}(t) \sim t^{\lambda_{mm}}, \tag{3.11a}$$

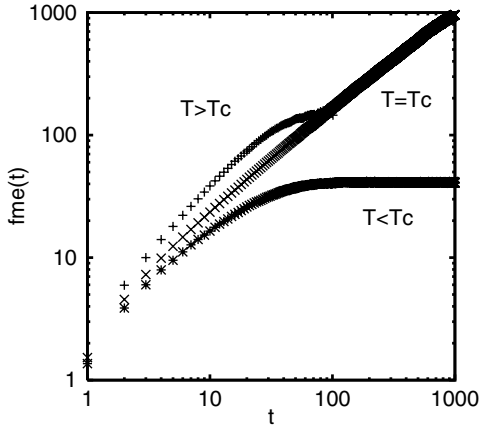

Figure 8. Typical behaviour of $f_{me}(t)$ corresponding to figure 7.

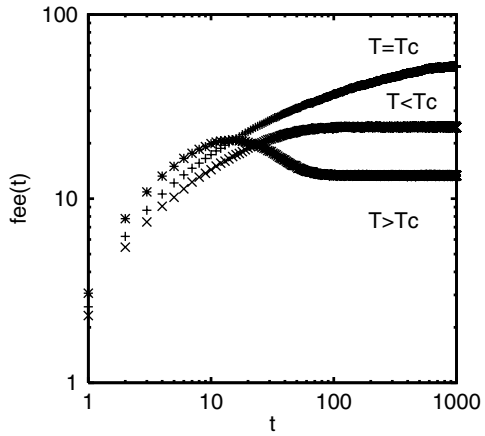

Figure 9. Typical behaviour of $f_{ee}(t)$ corresponding to figure 7.

$$f_{me}(t) \sim t^{\lambda_{me}}, \tag{3.11b}$$

$$f_{ee}(t) \sim t^{\lambda_{ee}}. \tag{3.11c}$$

The dynamical exponents are obtained from equations (3.4), (3.6) and (3.9) as

$$\lambda_{mm} = \frac{2\beta + \gamma}{z\nu} = \frac{d}{z}, \tag{3.12a}$$

$$\lambda_{me} = \frac{1}{z\nu}, \tag{3.12b}$$

$$\lambda_{ee} = \frac{\alpha}{z\nu}, \tag{3.12c}$$

where we use the hyper-scaling relation $\mathrm{d}\nu = 2\beta + \gamma$ in equation (3.12*a*).

As discussed in section 2.1, the total calculation time in a Monte Carlo simulation is proportional to the total number of updated spins $N_{\rm updated}$, which is related to the number of spins N, the number of samples for statistical averaging $N_{\rm av}$ and the maximum observation steps $t_{\rm max}$ as in equation (2.6). In equation (2.7), we mentioned that the statistical error for the averaged-order parameter $m(t)$ is proportional to $1/\sqrt{NN_{\rm av}}$. On the other hand, for the NER functions of fluctuations in equations (3.10*a*)–(3.10*c*), the statistical error $\Delta f(t)$ does not vanish even if $N \to \infty$ [53]. Actually, it is proportional to $1/\sqrt{N_{\rm av}}$. These functions are the fluctuations from sample to sample. This indicates

$$\Delta f(t) \propto \frac{1}{\sqrt{N_{\rm av}}} \tag{3.13}$$

for large enough systems. The statistical error for these functions can be set smaller as $N_{\rm av}$ is larger. This provides smaller system sizes N, and the crossover time $\tau(L)$ which should be larger than $t_{\rm max}$ becomes shorter. Thus, in contrast to the case of $m(t)$, large systems are not always preferable. If the CPU time is restricted and $t_{\rm max}$ is fixed, we need to find an optimal value of N (and $N_{\rm av}$).

3.2. Estimations of critical exponents

As an example, we estimated critical exponents for the FM Ising model in three dimensions [36, 37]. The simulation was performed at the critical temperature $T_{\rm c} = 4.511\,5158$ ($K_{\rm c} = 0.221\,6545$) estimated in [39]. The NER functions of fluctuations from an all-aligned state were calculated. Calculations were carried out on the $127 \times 127 \times 128$ simple-cubic lattice up to 1000 MCS. At each temperature, 2120 000 independent samples (time sequences) are used for statistical averaging up to 500 MCS, and so are 608 000 from 501 MCS to 1000 MCS. When the inverse temperature was changed within the range of $0.221\,580 \leqslant K \leqslant 0.221\,661$, deviations in the extrapolated values were within the error regions. The lattice with the size of $101 \times 101 \times 100$ was also simulated, but the finite-size effect was not observed.

Following the local exponent for the order parameter in equation (2.16), it is convenient to define local exponents for NER functions of fluctuations

$$\lambda_{mm}(t) = \frac{{\rm d}\log f_{mm}(t)}{{\rm d}\log t}, \tag{3.14a}$$

$$\lambda_{me}(t) = \frac{{\rm d}\log f_{me}(t)}{{\rm d}\log t}, \tag{3.14b}$$

$$\lambda_{ee}(t) = \frac{{\rm d}\log f_{ee}(t)}{{\rm d}\log t}. \tag{3.14c}$$

Functions of local exponents are often called the local exponent, too. For example, the local exponents corresponding to relations (2.13), (3.12*a*), (3.12*b*) and (3.12*c*) are defined as

$$z(t) = \frac{d}{\lambda_{mm}(t)}, \tag{3.15a}$$

$$\nu(t) = \frac{\lambda_{mm}(t)}{d \cdot \lambda_{me}(t)}, \tag{3.15b}$$

$$\beta(t) = \frac{\lambda_{m}(t)}{\lambda_{me}(t)}, \tag{3.15c}$$

$$\alpha(t) = \frac{\lambda_{ee}(t)}{\lambda_{me}(t)}, \tag{3.15d}$$

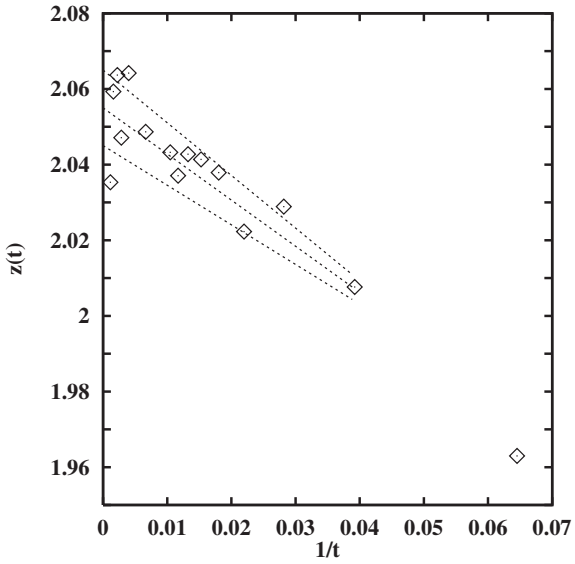

Figure 10. Local exponent $z(t)$ for the 3D FM Ising model [36, 37]. Three lines are extrapolated to $z = 2.045$, 2.055 and 2.065.

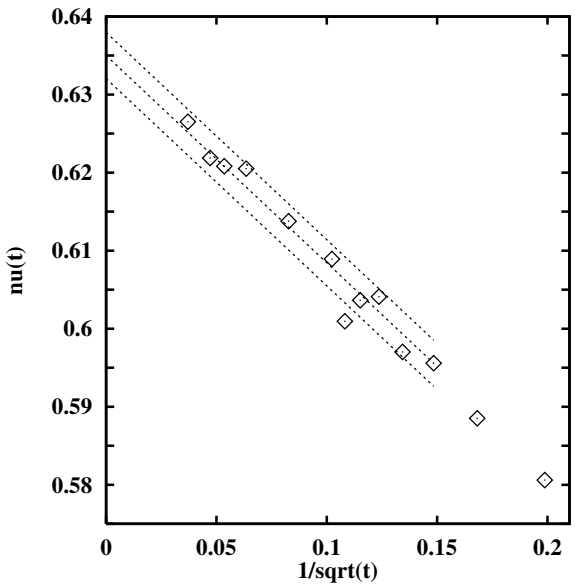

Figure 11. Local exponent $\nu(t)$ [36, 37]. The horizontal axis shows $1/t^{0.5}$. Three lines are extrapolated to $\nu = 0.632$, 0.635 and 0.638.

by which one can estimate each exponent directly from a plot versus $1/t$ like figure 3. The results are shown in figures 10–13.

The estimations of local exponents are examined by plotting them versus $1/t^{\Omega}$ for several values of Ω, and the asymptotic linear behaviour were observed when $\Omega = 1.0$ for $z(t)$, and

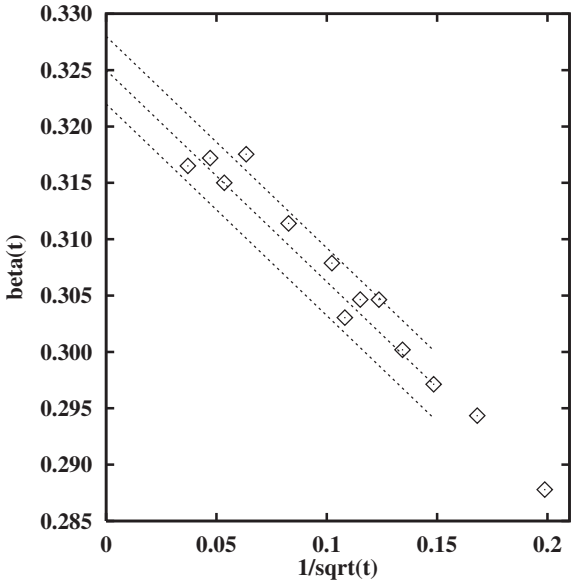

Figure 12. Local exponent $\beta(t)$ [36, 37]. The horizontal axis shows $1/t^{0.5}$. Three lines are extrapolated to $\beta = 0.320, 0.325$ and 0.330.

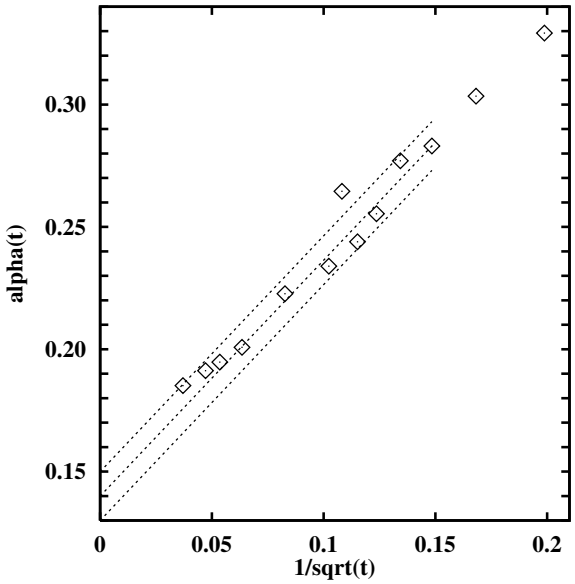

Figure 13. Local exponent $\alpha(t)$ [36, 37]. The horizontal axis shows $1/t^{0.5}$. Three lines are extrapolated to $\alpha = 0.13, 0.14$ and 0.15.

$\Omega = 0.5(1)$ for $\nu(t), \beta(t)$ and $\alpha(t)$. In figure 10, $z(t)$ is plotted versus $1/t$. The others in figures 11–13 are plotted versus $1/t^{0.5}$. These values of Ω are expected to be relating to exponents for the corrections to scaling [54]. Consequently, the exponents are estimated

as [36, 37]

$$z = 2.055(10), \qquad \nu = 0.635(5), \qquad \beta = 0.325(5), \qquad \alpha = 0.14(2). \tag{3.16}$$

Here the errors in the values of ν, β and α are a bit larger than the extrapolated values given in figures 11–13, because the ambiguity in correction exponent Ω is also taken into consideration. The estimation of z is consistent with the previous ones; 2.04(3) from the scaling analysis [55], 2.06(2) [28] and 2.05(2) [56] from the NER analysis, and 2.04(1) from the damage-spreading analysis [57]. The estimation of ν is larger than 0.6250(25) from the interface analysis [29] and 0.624(2) from the Monte Carlo renormalization group (MCRG) [46], but it is consistent with 0.6301(8) from the MCRG [47], 0.6289(8) from the scaling analysis [42], 0.6304(13) and 0.6305(25) from the perturbative RG analysis [58], and 0.630 02(23) from the high-temperature expansion (HTE) analysis [59]. The estimation of β is consistent with 0.324(4) from the magnetization analysis [43], 0.3258(44) from the scaling analysis [42], 0.3267(10) [47] and 0.3269(6) [48] from the MCRG, 0.3258(14) and 0.3265(15) from the perturbative RG analysis [58], and 0.32648(18) from the HTE analysis [59]. The estimation of $\alpha = 0.14(2)$ itself is a little bit larger than that obtained so far, while the corresponding $\nu = 0.620(7)$ derived from the hyper-scaling relation

$$\nu = \frac{2 - \alpha}{d} \tag{3.17}$$

is not so deviated from the direct estimation $\nu = 0.635(5)$.

The leading-order correction term was observed to be $1/t$ for $z(t)$, and it was $1/\sqrt{t}$ for $\nu(t)$ and $\beta(t)$. Therefore $\omega_t \geqslant 1$ and $\omega_\varepsilon/z = 0.5$ from equations (2.16), (3.10*a*) and (3.10*b*). Quantitatively speaking, the correction exponent ω_ε/z is estimated to be 0.5(1) from the present NER results. The correction exponent ω_ε was estimated [44] to be about 0.85. With the present NER estimation $z = 2.055$, ω_ε/z will be 0.41. The correction exponent ω_h was estimated to be about 2.07 [46], and therefore ω_h/z will be 1.0. These values are consistent with the present observation. It turns out that the NER analysis is also useful to study the correction behaviour.

3.3. Dynamical Rushbrooke's inequality

Although the NER approach for the estimations of critical exponents is successful in many systems [34–39, 50–52, 54, 60–65], only phenomenological arguments support it theoretically. Thus, exact theories concerning to this field are desirable to check the validity of the method. Here, we derive an exact inequality between the exponents λ_{mm}, λ_{me} and λ_{ee} [66], which is a dynamical extension for Rushbrooke's one [67].

Several decades ago, Rushbrooke proved an inequality for critical exponents in Ising systems using a thermodynamic identity [67],

$$\alpha + 2\beta + \gamma \geqslant 2. \tag{3.18}$$

It is general and extended to a wide variety of physical systems. This is called Rushbrooke's inequality. It is consistent with the scaling relation

$$\alpha + 2\beta + \gamma = 2, \tag{3.19}$$

which is derived from the scaling hypothesis for the free energy density

$$f(\varepsilon, h) = L^{(-2+\alpha)/\nu} g(L^{1/\nu}\varepsilon, L^y h), \tag{3.20}$$

where h is the external field. While equation (3.19) is not rigourous, together with the exact inequality (3.18) it has been playing an important role in statistical physics of phase transitions.

Let us consider arbitrary spin systems under the external field h. The starting point of Rushbrooke's proof [67] is the thermodynamic identity

$$C_h - C_m = T\left(\frac{\partial m_{\rm eq}}{\partial T}\right)_H^2 \Big/ \left(\frac{\partial m_{\rm eq}}{\partial h}\right)_T, \tag{3.21}$$

where C_h and C_m denote the specific heat under constant h and constant m, respectively. It is derived from the exact differential of entropy with respect to the temperature and the external field

$$\mathrm{d}S = \left(\frac{\partial S}{\partial T}\right)_h \mathrm{d}T + \left(\frac{\partial S}{\partial h}\right)_T \mathrm{d}h. \tag{3.22}$$

Since the specific heat is non-negative, equation (3.21) yields the inequality

$$C_h\left(\frac{\partial m_{\rm eq}}{\partial h}\right)_T \geqslant T\left(\frac{\partial m_{\rm eq}}{\partial T}\right)_h^2. \tag{3.23}$$

If the system undergoes a continuous phase transition at a definite transition temperature $T_{\rm c}$ and the spontaneous ordering (magnetization) appears below it, one can consider static critical exponents defined by

$$C_h \sim (-\varepsilon)^{-\alpha}, \tag{3.24a}$$

$$\left(\frac{\partial m_{\rm eq}}{\partial T}\right)_h \sim (-\varepsilon)^{\beta-1}, \tag{3.24b}$$

$$\left(\frac{\partial m_{\rm eq}}{\partial h}\right)_T \sim (-\varepsilon)^{-\gamma}. \tag{3.24c}$$

Then, equation (3.23) reveals Rushbrooke's inequality (3.18).

It is noted that equation (3.23) is nothing but a Schwartz's inequality. Let us denote the equilibrium correlation function for quantities A and B:

$$X(A, B) \equiv \langle AB\rangle_{\rm eq} - \langle A\rangle_{\rm eq}\langle B\rangle_{\rm eq}. \tag{3.25}$$

Since the positivity $X(A, A) \geqslant 0$ holds for any A, Schwartz's inequality is derived:

$$X(A, A)X(B, B) \geqslant X(A, B)^2. \tag{3.26}$$

Setting $A = \hat{m}$ and $B = \hat{e}$, one obtains an inequality

$$\left[\langle\hat{m}^2\rangle_{\rm eq} - \langle\hat{m}\rangle_{\rm eq}^2\right]\left[\langle\hat{e}^2\rangle_{\rm eq} - \langle\hat{e}\rangle_{\rm eq}^2\right] \geqslant \left[\langle\hat{m}\hat{e}\rangle_{\rm eq} - \langle\hat{m}\rangle_{\rm eq}\langle\hat{e}\rangle_{\rm eq}\right]^2, \tag{3.27}$$

which is equivalent to equation (3.23).

We consider an NER process starting from a fixed state, in which the dynamical average at time t is denoted by $\langle\cdots\rangle_t$. The correlation function in this dynamical process is defined by

$$X_t(A, B) \equiv \langle AB\rangle_t - \langle A\rangle_t\langle B\rangle_t. \tag{3.28}$$

Since the positivity $X_t(A, A) \geqslant 0$ is satisfied for any A and any t, Schwartz's inequality

$$X_t(A, A)X_t(B, B) \geqslant X_t(A, B)^2 \tag{3.29}$$

holds. Setting $A = \hat{m}$ and $B = \hat{e}$, one obtains an inequality

$$\left[\langle\hat{m}^2\rangle_t - \langle\hat{m}\rangle_t^2\right]\left[\langle\hat{e}^2\rangle_t - \langle\hat{e}\rangle_t^2\right] \geqslant \left[\langle\hat{m}\hat{e}\rangle_t - \langle\hat{m}\rangle_t\langle\hat{e}\rangle_t\right]^2, \tag{3.30}$$

for every t. This is a dynamical extension of inequalities (3.23) or (3.27).

While equation (3.30) is valid for any dynamical process, it is interesting to apply it to the process starting from a complete ordered state—the all-aligned state in the FM case—at

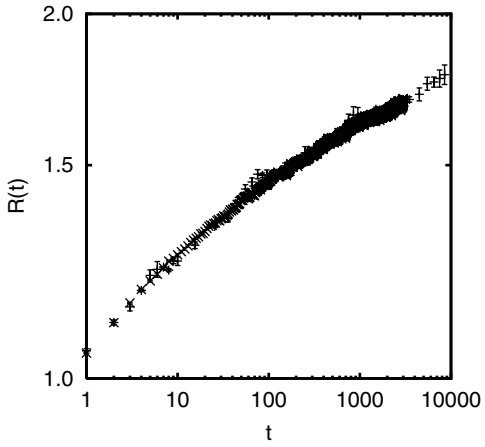

Figure 14. Numerically calculated $R(t)$ for the FM Ising model in three dimensions [66]. Double-log scale is used.

time $t = 0$. Using equation (3.30) together with equations (3.10*a*)–(3.10*c*), one obtains an inequality for NER functions

$$f_{mm}(t) f_{ee}(t) \geqslant f_{me}(t)^2, \tag{3.31}$$

which is the dynamical extension of equation (3.23) in this NER process [66]. Assuming the power-law divergence (3.11*a*)–(3.11*c*), one obtains the dynamical Rushbrooke's inequality

$$\lambda_{mm} + \lambda_{ee} \geqslant 2\lambda_{me}. \tag{3.32}$$

If one assumes the dynamic scaling hypothesis and equations (3.12*a*)–(3.12*c*), inequality (3.32) becomes identical with the original Rushbrooke's one (3.18).

It is valuable to see the behaviour of $R(t)$ defined by

$$R(t) \equiv \frac{f_{mm}(t) f_{ee}(t)}{f_{me}(t)^2} \tag{3.33}$$

in an NER analysis of fluctuations. This provides the validity of numerical calculations as well as the detail of asymptotic behaviour of NER functions in equations (3.11*a*)–(3.11*c*). In figure 14, we plot $R(t)$ for the FM Ising model on the simple cubic lattice at the transition temperature $T_c = 4.511\,5258$ ($K_c = 0.221\,6545$). The Metropolis Monte Carlo simulations are performed on the $381^2 \times 380$ lattice with skew boundary condition up to 10^4 MCS [66]. About 10^4 samples are used for averaging. It is shown that $R(t)$ is always greater than unity, which is consistent with equation (3.31).

In figure 14, the slope of the curve which indicates the power of relaxation seems nonzero and positive up to the observed MCS. If this keeps true in the asymptotic regime, $\lambda_{mm} + \lambda_{ee} - 2\lambda_{me}$ has a nonzero value. Because of equations (3.15*a*)–(3.15*d*), it reveals the broken of the scaling relation (3.19). However, we consider another explanation for this observation. In the previous subsection, the FM Ising model on the cubic lattice was analysed and obtained result (3.16) by the use of the NER of fluctuations [36, 37]. As pointed out there, the estimated values of z, ν and β are almost consistent with those obtained so far, while that of α is a little larger. It is natural to consider that the observation time is still short, and the asymptotic regime has not come. In fact, the curve shows a little convexity in figure 14, which indicates that the power would be decreasing in a longer time regime. Since

only the estimated α gives a remarkable deviation, the convergence speed to the asymptotic regime, which is relating to the corrections to scaling, is different among NER functions. It is expected that the convergence speed of the function $f_{ee}(t)$ is much slower than those of others. At present, we have no idea to explain this phenomenon. Further investigations would be necessary in future.

4. First-order phase transition

The first-order phase transition appears frequently in nature; e.g. in the liquid–gas transition, in the FM Potts model with $q \geqslant 5$ in two dimensions and so on. A typical property in such systems is the hysteresis phenomenon. If one sets the initial state of relaxation as one of the ordered states, the order parameter approaches a finite value even above the transition temperature, which is called the super heating. On the other hand, if the initial state is a randomly oriented state which corresponds to the infinite temperature limit, the order parameter decays to zero even below the transition temperature, which is called the super cooling. To complete the NER method as a standard analysis of phase transitions in statistical physics, it should be applied to first-order transition systems.

4.1. Hysteresis phenomenon

The NER method has already been applied partly to first-order transition cases [68]. That is the confirmation of weak first-order transition. In last decades, the numerical confirmation of weak first-order transition has been one of the fascinating problems in statistical physics [69–74]. Since the correlation length becomes very large but finite at the transition point, it is difficult to distinguish it with the second-order one by numerical simulations with relatively small finite lattices. In the NER analysis, observing the hysteresis phenomenon, one can confirm the first-order transition even it is a weak one, i.e. estimating the transition temperatures both with heating and cooling processes and check the discrepancy of them. Since these estimations are precisely made on large lattices in the NER analysis, the method can be applied even to a weak first-order transition case in which the discrepancy is very small.

Let us see an example of the hysteresis in an NER process using the q-state FM Potts model in two dimensions

$$H = -J \sum_{\langle ij \rangle} \delta_{S_i, S_j}, \tag{4.1}$$

where the spin variable S_i takes $1, 2, \ldots, q$. The summation is taken over all nearest neighbouring pairs on the square lattice. Using the duality relation with an assumption of unified transition point, one can evaluate the transition temperature for general q from the self-dual point on the square lattice [75], i.e.

$$T_0(q) = \frac{1}{\log(\sqrt{q}+1)}. \tag{4.2}$$

It is expected that the transition is of second order for $q \leqslant 4$ and is of first order for $q > 4$. In the case of $q = 5$, the first-order transition occurs but the latent heat is very small; the correlation length becomes very long at around the transition temperature. That is called the weak first-order transition [69–74]. On the other hand, for large q, a remarkable hysteresis appears, and the true transition temperature becomes hard to evaluate numerically. Here, we treat the $q = 20$ case, in which a relatively large hysteresis appears. From equation (4.2), the true transition temperature for $q = 20$ is expected as

$$T_0(20) = 0.588\,3498\ldots. \tag{4.3}$$

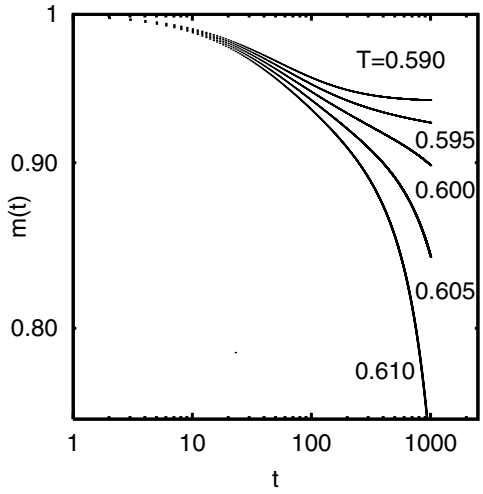

Figure 15. Relaxation of order parameter $m(t)$ for the 2D $q = 20$ FM Potts model in the heating process [76].

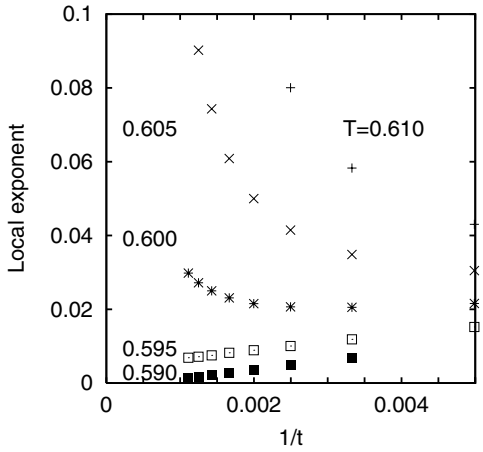

Figure 16. Local exponent of $m(t)$ corresponding to figure 15 is plotted for $q = 20$ in the heating process [76]. The transition temperature is estimated as $T_{\text{heat}} = 0.5975(25)$.

First, we show the order parameter relaxation from an ordered initial state [76] in figure 15. It corresponds to the heating process. We initialize all spins as $S_i = 1$ and estimate the order parameter

$$m(t) = \frac{1}{N} \sum_i \left\langle \frac{q\delta_{S_i,1} - 1}{q - 1} \right\rangle_t . \tag{4.4}$$

This function vanishes in the PM phase and remains finite in the FM phase. Calculations are carried out on 2001×2000 square lattice with skew boundary condition. About 320 independent samples are taken for statistical averaging at each temperature. From the date in figure 15, we plot the local exponent (2.16) for the heating process in figure 16. In

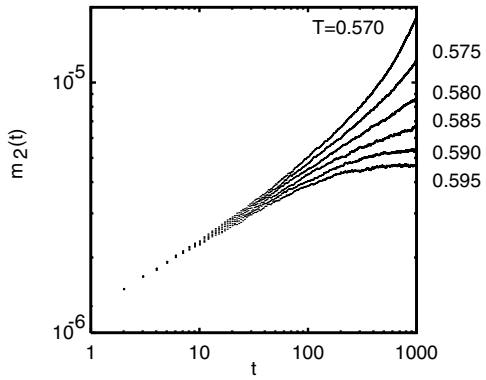

Figure 17. Relaxation (evolution) of order parameter $m_2(t)$ for the 2D $q = 20$ FM Potts model in the cooling process [76]. The transition temperature is estimated as $T_{\rm cool} = 0.580(5)$.

$T \geqslant 0.600$, $\lambda(t)$ seems to diverge for large t indicating the PM phase. It seems to be vanishing in $T \leqslant 0.595$ indicating the FM phase. Thus, the transition temperature in the heating process is estimated as

$$T_{\rm heat} = 0.5975(25). \tag{4.5}$$

Note that this estimation does not indicate the true transition temperature (4.3) but its upper bound because of the hysteresis.

Next, we calculated the order parameter relaxation from a disordered initial state [76]. It corresponds to the cooling process. We initialize all spins randomly. Since the initial state is symmetric in the q states, we need to analyse an invariant-order parameter to this symmetry like the squared magnetization in the FM Ising case. Let us consider the unit vector $\mathbf{e}(\alpha)$ $(\alpha = 1, \ldots, q)$ pointing in the q symmetric directions of a hyper-tetrahedron in $q - 1$ dimensions, and assign it to the spin state $S_i = \alpha$. In this formulation, the delta function is written as

$$\delta_{S_i,S_j} = \frac{1}{q}[1 + (q-1)\mathbf{e}(S_i) \cdot \mathbf{e}(S_j)]. \tag{4.6}$$

Then, we define the order parameter as

$$m_2(t) = \frac{1}{N^2}\left\langle \left| \sum_i \mathrm{e}(S_i) \right|^2 \right\rangle_t. \tag{4.7}$$

The behaviour of this quantity is similar to the susceptibility. It approaches a finite value of $O(N^{-1})$ in the PM phase and diverges (approaches an $O(1)$ value) in the FM phase. Calculations were carried out on 1001×1000 square lattice. About 2048 independent samples are taken for statistical averaging at each temperature. The result is plotted in figure 17. Note that the data are somehow ramified, since the statistical error is relatively large in the cooling process up to the present observation time. This comes from the fact that the magnitude of the order parameter in the cooling process, which evolves from zero, is much smaller than that in the heating process, which decays from unity. In $T \geqslant 0.585$, $m_2(t)$ seems to remain finite indicating the PM phase. It seems to be diverging in $T \leqslant 0.575$ indicating the FM phase. The behaviour at $T = 0.580$ is not distinguishable in this time scale. Thus, the transition temperature in the cooling process is estimated as

$$T_{\rm cool} = 0.580(5). \tag{4.8}$$

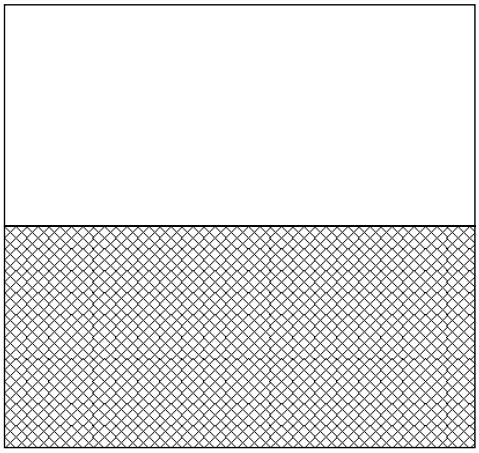

Figure 18. Schematic diagram of the mixed phase initialization (MPI). The (complete) ordered initial state in the upper side and a random initial state in the lower side are merged.

This is a lower bound of the true transition temperature. Clearly, we observe the hysteresis in the range of $0.580 < T < 0.5975$ with respect to the true transition point (4.3).

4.2. Mixed phase initialization

While the extension of the NER method is successful for the confirmation of weak first-order transition [68, 76], the most important problem, the estimation of true transition temperature, has remained unsettled because of the hysteresis phenomenon. At the transition temperature, several thermodynamic phases coexist, and their equilibrium free energies coincide with each other. At a glance, it is difficult to find such a point defined by the balance of equilibrium quantities from the nonequilibrium process. Therefore, it was proposed that the centre of upper and lower bounds estimated by the above-mentioned two initial conditions is an approximate transition temperature. In the case of weak first-order transition, it is not so bad approximation since the range of hysteresis is very small, while, in the normal first-order transition case, there is no reason to take it as a good one. In fact, in the mean field Potts model, one can easily find that the centre point is quite deviated from the true transition temperature.

To estimate the true transition temperature from a relaxation process, we use another initial state called the mixed phase initialization (MPI) [76–78]. Let us consider a spin configuration in which spins in upper-half lattice are initialized as $S_i = 1$ and those in lower-half lattice are initialized randomly (see figure 18). Both ordered and disordered clusters coexist with equal weight. The boundary between these regimes is completely flat at initial. In general first-order transitions, the initial state for the MPI may consist of several number of clusters, each of which is in one of the stable states at the transition point.

Let us check the validity and efficiency of MPI for the $q = 20$ case [76]. In figure 19, we show the relaxation of order parameter $m(t)$ with MPI. Calculations were carried out on a 2001×2000 square lattice. About 320 independent samples are taken for statistical averaging. The corresponding local exponent is plotted in figure 20. In $T \geqslant 0.5885$, $\lambda(t)$ seems to diverge for large t indicating the PM phase. It seems to be vanishing in $T \leqslant 0.588$ indicating the FM phase. Thus, the transition temperature with MPI is estimated as

$$T_{\mathrm{mix}} = 0.588\,25(25), \tag{4.9}$$

which is close to the true value (4.3).

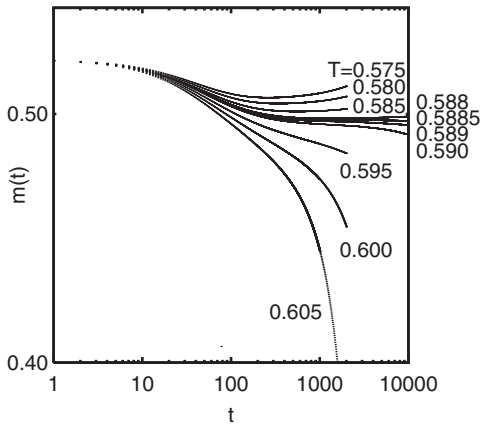

Figure 19. Relaxation of $m(t)$ for the 2D $q = 20$ FM Potts model with the MPI [76].

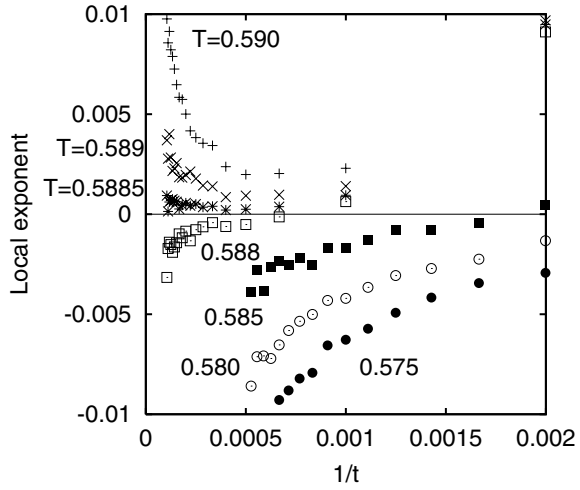

Figure 20. Local exponent of $m(t)$ corresponding to figure 19 is plotted for $q = 20$ with the MPI [76]. The transition temperature is estimated as $T_{\rm mix} = 0.588\,25(25)$.

The same analysis was made for $q = 5$ case, which is the most weak first-order one in this model [76]. In figure 21, the local exponent is plotted. In $T \geqslant 0.8516$, $\lambda(t)$ seems to diverge for large t and vanishes in $T \leqslant 0.8515$. Thus, the transition temperature is estimated as $T_{\rm mix} = 0.85155(5)$ which is also close to the exact value $T_0(5) = 0.851\,5284\ldots$. The difference of these two cases in the MPI analysis is the exponent λ_m around the transition point. For $q = 20$ case, it is almost zero indicating no power-law decay, which is consistent with the finite correlation length at the transition point. For $q = 5$ case, it seems to point a finite value ($\sim$0.02) indicating a power-law decay. This is due to the weak first-order transition. The system behaves like a second-order transition in shorter time. It is expected to crossover to zero in longer time, while we cannot observe it. Anyway, the transition temperature can be resolved precisely in this time scale by the point between diverging and vanishing behaviour.

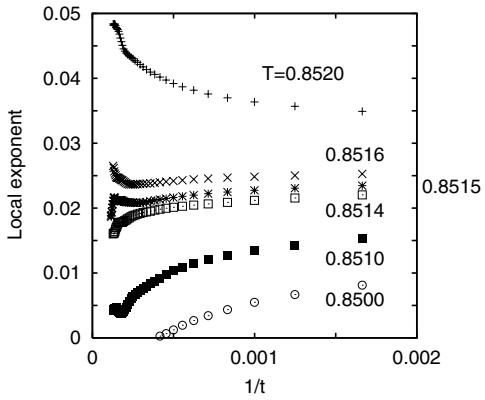

Figure 21. Local exponent of $m(t)$ for the 2D $q = 5$ FM Potts model with the MPI [76].

As shown above, the NER analysis with MPI provides a precise estimation of transition temperature for first-order transition systems. To understand this mechanism, we discuss the cluster growth around the transition temperature T_0. First, we consider the heating process, in which the system is initialized to an ordered state. For the temperature just above T_0, the ordered state becomes metastable and the disordered state is the globally stable state. Thus, the super saturation phenomenon is observed in the heating process. The bulk free energy decreases if the system transfers to a disordered state. To realize this transfer, clusters of disordered state appeared in the bulk-ordered regime evolves infinitely. Let us consider the dynamics of a disordered cluster of a length scale L in an ordered regime. The free energy change with respect to the cluster growth of $L \to L + \mathrm{d}L$ is written as

$$\mathrm{d}F = A(L)\,\mathrm{d}L. \tag{4.10}$$

The coefficient $A(L)$ is called the affinity and is expressed as

$$A(L) = L^{d-2}\sigma - L^{d-1}\Delta f, \tag{4.11}$$

where σ is the interface tension between these two phases. The free energy difference is defined by

$$\Delta f \equiv f_{\mathrm{o}} - f_{\mathrm{d}}, \tag{4.12}$$

where f_{d} and f_{o} are per spin free energy in disordered and ordered phases, respectively. Clearly, $f_{\mathrm{o}} > f_{\mathrm{d}}$ holds in $T > T_0$. The cluster shrinks when $A(L) > 0$, while it evolves infinitely and the system transfers to a stable state when $A(L) < 0$. There exists a critical length scale

$$L_{\mathrm{c}} \sim \frac{\sigma}{\Delta f} \tag{4.13}$$

defined by $A(L_{\mathrm{c}}) = 0$. It becomes larger if the temperature is closer to T_0. To realize a stable phase, it is necessary for the system to nucleate a cluster larger than L_{c} by thermal fluctuation. In the first-order transition case, the free energy difference vanishes $\Delta f \to 0$ as $T \to T_0$, while the interracial tension σ remains finite. Thus, $L_c \to \infty$ for $T \to T_0$, and the nucleation of clusters larger than L_{c} becomes hard around the transition point. This causes the super heating and leads to hysteresis. The same argument can be made for the temperature just below T_0 in the cooling process.

For the MPI case, infinite clusters of ordered and disordered phases exist simultaneously at initial. Both above and below T_0, a cluster of the stable phase larger than L_c has been prepared initially. In this case, the surface free energy does not change with the evolution of the stable cluster since the surface area does not so change as compared with its volume. Therefore, the system always transfers to a global stable state irrespective of temperature. One can distinguish the phase by the criterion like equations (2.2) or (2.21). It is not necessary to take care of the exponent at the transition point, since it is not used in the estimation. The fact that the ratio of volumes for two initial clusters is unity is not taken seriously. It may be $1/2$ or $1/3$ or something not too small one, while we choose it as it is for convenience.

5. What is the advantage of the NER method?

The most NER analysis is based on the Monte Carlo dynamics, which is identical with the standard EMCS. The data in equilibration, which is discarded in EMCS, are used for the analysis. The EMCS is widely used in statistical physics, since the coding for the Markovian process with the transition rate which satisfies the detailed-balance condition is simple and straightforward to apply many kinds of systems. It has revealed many helpful information on phase transitions and critical phenomena. These features are the same in the NER method.

In most EMCS, analyses are made with the finite size scaling hypothesis and resulting scaling plots providing the transition temperature as well as critical exponents. However, the EMCS is sometimes confronted with difficulties in the case of the so-called 'slowly relaxing systems'. In a low-temperature regime of frustrated systems or in critical regime of some low-dimensional systems, the relaxation becomes tremendously slow, and the simulation takes much time for equilibration. The total amount of calculation time consists of equilibration and averaging, and it is proportional to the equilibration time, since, in usual, the averaging time is taken several times of the equilibration one. The equilibration from a fixed nonequilibrium state is achieved when the spin correlation $\xi(t)$ grows up to the scale of the equilibrium correlation length ξ_{eq} or the system size L. In the critical regime, since the correlation length becomes larger than simulated sizes, the equilibration time becomes longer as the system size is larger. Therefore, available system sizes are restricted too small in slowly relaxing systems, which prevent accurate estimations for the critical point and critical exponents. If the equilibration time is not sufficient, one sometimes suffers a serious error, called 'systematic error', in the data and mislead the result. The importance sampling is used for statistical averaging in EMCS, in which equilibrium ensemble is generated by a time sequence. Thus, the sampling is not completely independent, which would causes the systematic error. The development and improvement of simulation technique in last decades are mainly devoted to overcome this difficulty.

On the other hand, in the NER method, the statistical averaging is performed by the independent sampling of time evolution. Since the equilibration is not necessary in the simulation, it is not necessary to wait a long time for that even in slowly relaxing systems. Therefore, one does not need to be anxious about such systematic errors. This feature is effective more in frustrated and/or random systems in which the slow relaxation appears frequently.

In the NER analysis for second- (or first-)order transitions, as discussed in section 2.1, one may choose the system size as large as possible; usually it is restricted by the storage size. Therefore, one can analyse the data which can be recognized as in the thermodynamic limit up to the maximum observation time; to do so, one needs to check the size dependence of the data. The limitation is taken for the size, and analysis is made on the finite-time data. Of course, such finite-time data are not in equilibrium. It is necessary to use the criterion

like equation (2.2) or the finite time scaling (2.11). Furthermore, the confirmation of the asymptotic relaxation in the NER analysis is not always easy for some complicated systems. This strategy is opposite to the analysis in EMCS, in which the limitation is taken for the time, and analysis is made on the finite-size data. Finite time or finite size? This is a trade-off between these numerical investigations. In some cases, both work well, while, in slowly relaxing systems, the latter sometimes suffers the systematic errors.

To estimate the transition temperature T_c in EMCS numerically, a theoretical relation is often used which holds just at $T = T_c$. The NER method introduced in section 2 or section 4 is much different from that. It is estimated between the upper bound as the minimum temperature observed in the disordered phase and the lower bound as the maximum temperature observed in the ordered phase. We do not estimate T_c directly, but identify the phase at each temperature observing the NER of order parameter step by step and then determine the estimation of T_c as the temperature region where we cannot identify the phase clearly. At each temperature, the identification of the phase is easily performed by the local exponent through criterion (2.21). Therefore, the results in the NER analysis are much precise. If one needs a higher accuracy, he may observe the NER of order parameter with a higher resolution of temperatures around $T = T_c$, in which longer time simulations would be necessary to identify the phase.

The NER analysis has been used successfully to study various problems including frustrated and/or random systems. The frustrated system is one of the main subjects in statistical physics [79, 80] because of its rich phase diagrams possibility of new universality classes and slow dynamics in the relaxation. In the following, we show some successful example of the NER analysis for such systems.

5.1. Application: chiral transition

The NER method works efficiently to study the systems which show the so-called 'exotic phase transition'. The NER analysis has been successful for the chiral transition in the fully frustrated (FF) XY models in two dimensions [64, 65, 81], i.e. the antiferromagnetic (AF) XY model on the triangular lattice and the FFXY model on the square lattice. It is noted that these systems include typical frustrations. The order parameter of the chiral phase is hidden in the Hamiltonian of the system, while the result manifests that the NER analysis is not disturbed by this fact.

We have investigated both the FFXY model on the square lattice [72, 82–98] and the AFXY model on the triangular lattice [72, 83–85, 98–102]. In these models, the possibility of two different transitions, the chiral transition and the KT one, has been discussed (this point will be mentioned in a later section). A controversy arose concerning to the universality class for the chiral transition [100]. Since the broken symmetry in the chiral transition is a discrete Z_2 one, which is the same as the Ising model, it is natural to expect that the universality class is in the 2D Ising class ($\nu = 1, \beta = 1/8 \cdots$). However, some numerical studies indicated different classes [72, 89, 91, 92, 102].

The Hamiltonian we have considered is

$$\mathcal{H} = -J \sum_{\langle ij \rangle} \cos(\theta_i - \theta_j + A_{ij}), \tag{5.1}$$

where $J > 0$ and $0 \leqslant \theta_i \leqslant 2\pi$. The summation $\langle ij \rangle$ is taken over all nearest neighbouring sites on the square or triangular lattices. The constant A_{ij} takes π for all bonds for the triangular-lattice system, which represents nothing but an AF interaction. For the square-lattice system, it takes 0 for three of four bonds on a plaquette and π for the other one. The ground states for these model have spin structures with clockwise or counterclockwise rotation on each plaquette in two subplaquette patterns. The angular difference is $\pi/4$ for the square-lattice

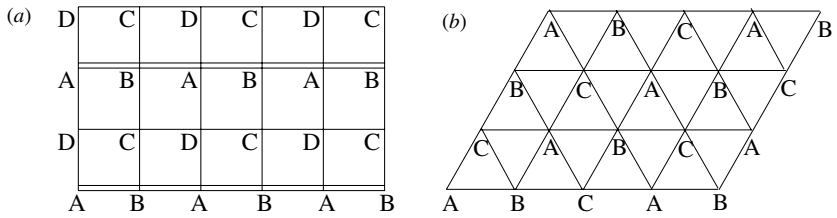

Figure 22. Initial states for NER analysis (*a*) for the square-lattice case and (*b*) for the triangular-lattice case. They are one of the ground states with $\kappa = m = 1$ for each model. For the square lattice, the double line indicates the AF interaction and others are the FM ones.

system, and $2\pi/3$ in the triangular-lattice one. The system has a Z_2 symmetry due to this clockwise–counterclockwise degeneracy and a continuous $U(1)$ symmetry due to the global rotational symmetry with respect to the spin orientation. Thus, in a low-temperature regime, two kinds of phases appear. One is the KT phase associated with the $U(1)$ symmetry in two dimensions and the chiral phase associated with the Z_2 symmetry.

In the NER analysis, the initial state of relaxation is chosen as one of the ground states. That is a four-sublattice structure in the square-lattice system ($\theta_A = 0, \theta_B = \pi/4, \theta_C = \pi/2$ and $\theta_D = 3\pi/4$), and a three-sublattice structure in the triangular-lattice one ($\theta_A = 0, \theta_B = 2\pi/3$ and $\theta_C = 4\pi/3$). They are illustrated in figures 22(*a*) and (*b*). Let us denote the initial values as θ_i^0. In the present case, we need to calculate two kinds of order parameters at each time t, the chiral-order parameter

$$\kappa(t) = \frac{a}{N} \sum_{(i \to j)} \langle \sin[\theta_i(t) - \theta_j(t)] \rangle_t, \tag{5.2}$$

which is the z-component of the vector chirality [82, 99], and the spin orientational order parameter

$$m(t) = \frac{1}{N} \sum_i \left\langle \cos\left[\theta_i(t) - \theta_i^0\right] \right\rangle_t, \tag{5.3}$$

which detects the ordering with respect to the $U(1)$ symmetry. The summation for $(i \to j)$ is taken for all bonds with a fixed direction, (A $\to$ B $\to$ C $\to$ D $\to$ A or A $\to$ B $\to$ C $\to$ A) and a is a normalization factor as $a = 1/\sqrt{2}$ or $a = 2/3\sqrt{3}$. The initial states in figures 22(*a*) and (*b*) give $m(0) = \kappa(0) = 1$. The analysis for the latter-order parameter (5.3) is discussed in section 6.3.

As an example of calculations for the chiral-order parameter, we show the result for the FFXY mode on the square lattice [64, 65] in figure 23. Calculations are carried out on a 2000×2000 lattice up to the observation time 5000 MCS. About $320 \sim 2800$ independent runs are performed for averaging. The size dependence is checked to be negligible, when we compare the data with those on a 1500×1500 lattice for some temperatures. In figure 23, the chiral transition temperature $T_c = 0.4535(5)$ is clearly indicated. It is seen that the analysis is succeeded as for the FM Ising model. The same analysis is made for the AFXY model on the triangular lattice and obtain the chiral transition temperature $T_c = 0.512(1)$.

Next we made the NER analysis of fluctuations for the chiral transition [64, 65]. Calculations are made at $T_c = 0.4535$ on a 500×500 square lattice and at $T_c = 0.512$ on a 500×501 triangular lattice up to the observation time 500 MCS. About 10^6 independent runs are performed for averaging. The size dependence is checked to be negligible by comparing the data with 800×800 or 800×801 lattices. In figure 24, the local exponents for z and ν are shown, which correspond to figures 10 and 11. They are plotted versus $1/t^{\Omega}$, which is

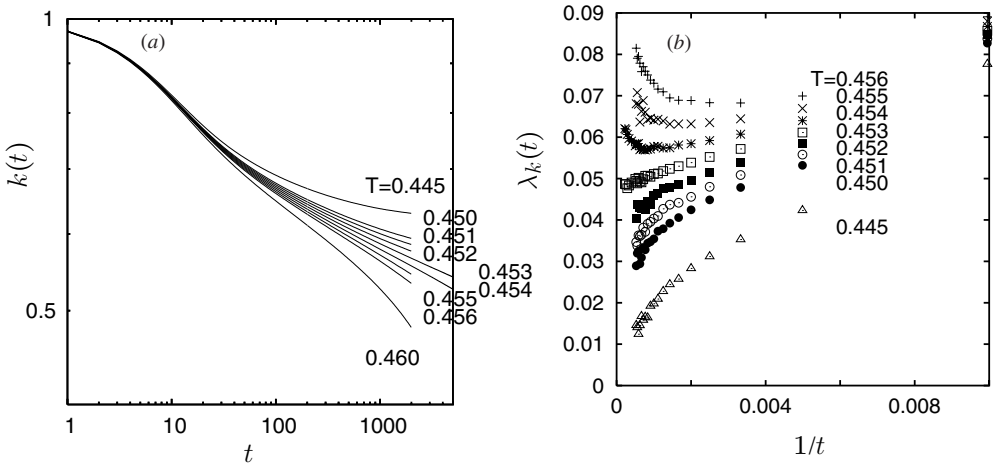

Figure 23. (*a*) Relaxation of chiral-order parameter $\kappa(t)$ in a double-log plot for the square-lattice system and (*b*) the corresponding Local exponent [64, 65]. This provides the chiral transition temperature $T_c = 0.4535(5)$.

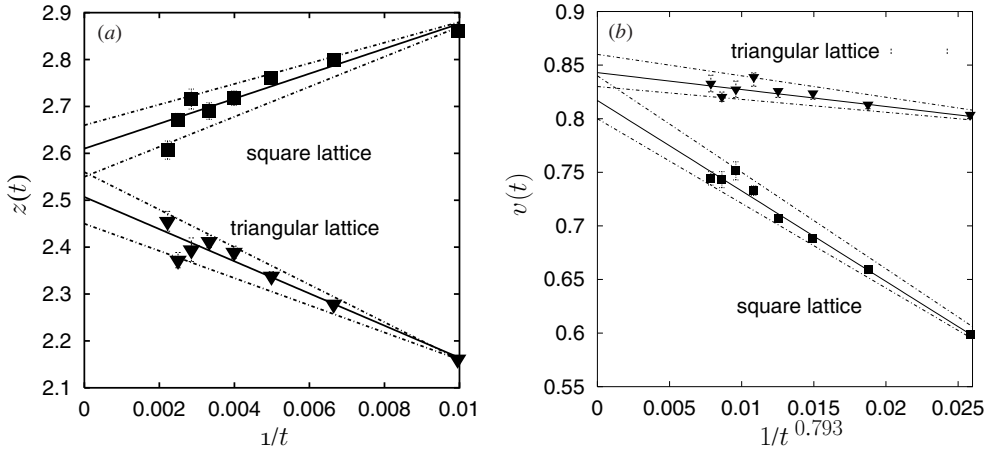

Figure 24. (*a*) Local exponent $z(t)$ and (*b*) $\nu(t)$ at $T_c = 0.4535$ for the square-lattice system and at $T_c = 0.512$ for the triangular-lattice system [64, 65].

chosen so that the linearity becomes best in the extrapolation. The results are summarized in table 1. The result indicates that the chiral transition in the 2D FFXY models belongs to the same universality class including the dynamical behaviour. It is different from the 2D Ising one in which $\nu = 1$ and $\beta = 1/8$. The values of z are larger than that in the pure Ising model ($z \sim 2.06$) [28] indicating the slow relaxation due to frustration.

5.2. Application: multi-critical point and random fixed point

We also investigated a frustrated and random system, the $\pm J$ Ising model in two and three dimensions, and examine the effect of randomness on the FM critical phenomenon. The

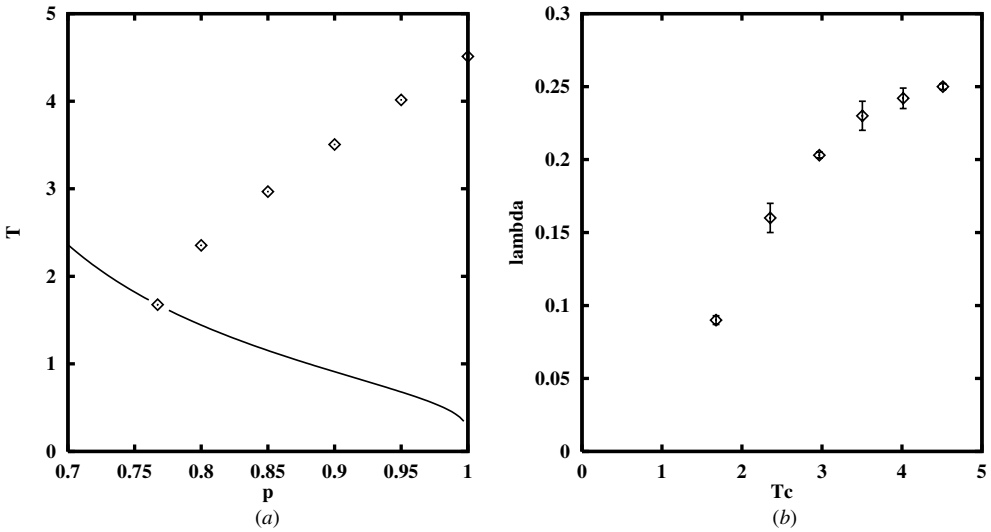

Figure 25. (*a*) FM transition points for the 3D $\pm J$ Ising model are plotted in the $p - T$ plane [110]. The solid curve shows the Nishimori line. (*b*) Corresponding exponent λ_m is plotted as a function of the transition temperature [110].

Table 1. Summary of chiral transition temperatures and critical exponents for the FFXY models [64, 65].

Lattice	T_c	ν	β	η	z
Square	0.4535(5)	0.851(25)	0.112(7)	0.28(3)	2.48(8)
Triangular	0.512(1)	0.845(25)	0.105(8)	0.26(3)	2.51(7)

Hamiltonian is

$$\mathcal{H} = -\sum_{\langle ij \rangle} J_{ij} S_i S_j, \tag{5.4}$$

where the summation runs over all nearest neighbour sites on d-dimensional hyper-cubic lattices. The exchange interaction J_{ij} is an independent random variable. It takes $J(> 0)$ with probability p, or $-J$ with probability $(1 - p)$. The behaviour of this model along the so-called Nishimori line [103],

$$2K = \log \frac{p}{1-p}, \tag{5.5}$$

is well studied, where $K = J/k_B T$. The multi-critical point (MCP) where the PM, the FM and the SG (if it exists) phases merge is considered to be located on this line [103–109]. The specific heat does not diverge on this line, providing $\alpha \leqslant 0$.

The MCP has been located finely with the NER analysis [38, 62, 63, 110, 111]. It is obtained by the calculation of magnetization $m(t) \equiv [\langle m \rangle_t]_c$ along the Nishimori line [111], where $[\cdots]_c$ denotes the average for randomness. The MCP is estimated as $p_{mc} = 0.7673(3)$ with $\lambda_m = 0.090(3)$ in 3D (on the simple cubic lattice) and $p_{mc} = 0.8894(9)$ with $\lambda_m = 0.021(1)$ in 2D (on the square lattice). Other transition points on the FM boundary are also estimated with p-fixed. The FM phase boundary and corresponding dynamic critical exponent $\lambda_m = \beta/z\nu$ in 3D are obtained as in figure 25 [110]. It is confirmed that $\beta/z\nu$ is

Table 2. Summary of transition temperatures and critical exponents for the 3D $\pm J$ Ising model [62, 63].

p	K_c	ν	β	z
1.00	0.2216454(15)	0.635(5)	0.325(5)	2.055(10)
0.90	0.285285(5)	0.70(3)	0.36(1)	2.16(4)
0.80	0.4251(1)	0.69(2)	0.335(5)	3.10(3)
0.78	0.4925(2)	0.70(2)	0.34(1)	3.75(5)
$p_{mc} = 0.7673$	0.5966(8)	0.88(2)	0.41(1)	5.1(1)

Table 3. Summary of transition temperatures and critical exponents for the 2D $\pm J$ Ising model.

p	T_c	ν	β	z
1.00	$2.269\cdots$	1	0.125	2.165(10)
0.98	2.11979(67)	1.00(4)	0.129(5)	2.32(11)
0.96	1.96078(38)	1.00(4)	0.129(5)	2.44(11)
0.94	1.7857(32)	1.03(3)	0.130(5)	2.68(14)
0.92	1.5823(25)	1.05(5)	0.131(6)	3.06(16)
0.898(1)	1.27389	1.14(9)	0.135(13)	3.94(18)
$p_{mc} = 0.8899$	0.9571	1.25(6)	0.114(6)	5.7(2)

non-universal and varies from the pure case to the MCP. The same behaviour is observed also in two dimensions. What is the origin of this non-universal behaviour? If it is due to the dynamical effect, only the exponent z could be non-universal.

It was suggested by MCRG study [104] that the static exponents along the boundary of FM transition are not much different from those of the pure system—universality—except the MCP, and so do the ratio of them (β/ν, γ/ν)—weak universality—including the MCP. The series expansion study [106] concluded that $\nu = 0.85(8)$ and $\gamma = 1.80(15)$ at the MCP belong to a different universality class from that at the pure FM case ($\nu = 0.630$ and $\gamma = 1.24$). Hukushima [112] investigated the phenomenological MCRG based on numerically calculated domain-wall free energies in the $p-T$ plane. His result suggests the existence of the so-called random fixed point. This means that a single universality class would hold along the FM phase boundary in $p_{mc} < p < 1$, and at least three universality classes exist for FM transitions; the pure case, the random fixed point and the MCP.

To discuss the origin of non-universal behaviour of $\beta/z\nu$, we have estimated z, ν and β using the NER of fluctuations [62, 63]. Calculations were carried out for several points on the phase boundary listed in table 2 with the size of $151 \times 151 \times 152$. At each point, we choose 2×10^7–2×10^8 independent Monte Carlo runs for averaging. The local exponents defined by equations (3.15*a*)–(3.15*c*) are plotted in figure 26, and resulting exponents are listed in table 2. The estimated exponents at the MCP, $\nu = 0.88(2)$ and $\beta = 0.41(1)$, are consistent with those obtained by the series expansion [106], if we use the hyper-scaling relation, $2\beta + \gamma = d\nu$. It is also consistent with the non-divergence of the specific heat, since $\alpha = 2 - d\nu = -0.64(6)$. It is observed that the estimations of z are almost different from each other. Thus, it is found that the non-universal behaviour of $\beta/z\nu$ is due to that of z. It is observed that estimations of ν in $p_{mc} < p < 1$ show almost the same value around $\nu = 0.70$, which is different from the estimation $\nu = 0.88(2)$ at $p = p_{mc}$ as well as the estimation $\nu = 0.635(5)$ at $p = 1$. A similar behaviour is observed for the result of β. This indicates the existence of three classes of universality and the random fixed point in three dimensions.

The same analysis is made for the two-dimensional case. [113]. Calculations are carried out for several points on the phase boundary listed in table 3 with the size of 1001×100. At

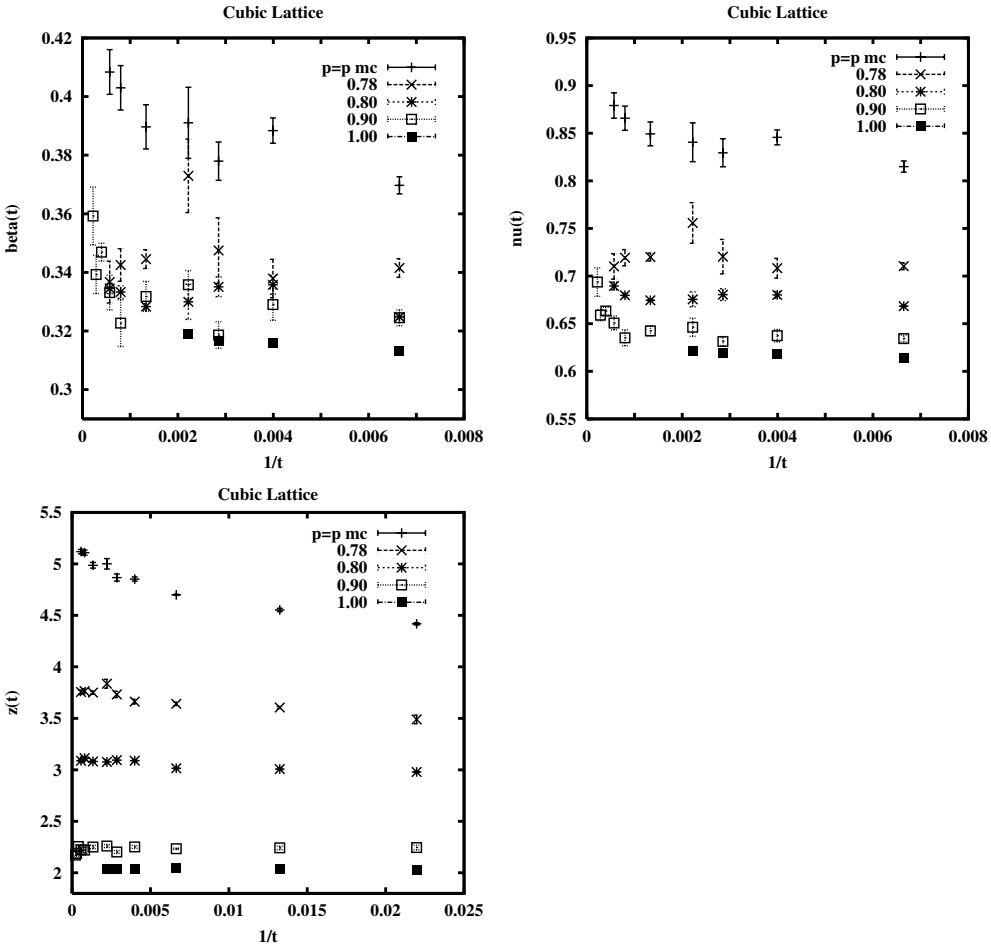

Figure 26. Local exponent $\beta(t)$, $\nu(t)$ and $z(t)$ for the 3D $\pm J$ Ising model [62, 63].

each point, we choose 4×10^5–6×10^5 independent Monte Carlo runs for averaging. The local exponents defined by equations (3.15*a*)–(3.15*c*) are plotted in figure 27; resulting exponents are listed in table 3. The estimations of z are almost different from each other. Thus, the non-universal behaviour of $\beta/z\nu$ is due to the non-universal behaviour of z, which is the same behaviour as in three dimensions. It is observed that estimations of ν in $p_{\rm mc} < p \leqslant 1$ (including $p = 1$) show almost the same value around $\nu = 1.0$, which is different from the estimation $\nu = 1.25(2)$ at $p = p_{\rm mc}$. A similar behaviour is observed for the result of β. This indicates that only two classes of universality appear and the random fixed point does not exist in two dimensions, which is different from the three-dimensional case.

6. Kosterlitz–Thouless transition

The Kosterlitz–Thouless (KT)[4] [114–117] is one of the examples to show a remarkable slow relaxation which causes a difficulty in numerical simulations. In two dimensions, there exists

[4] While the nature of the phase transition and the character of the low temperature phase in the ferromagnetic XY model were first established by Berezinskii [114, 115], I call this phase the KT one since it is familiar in the society.

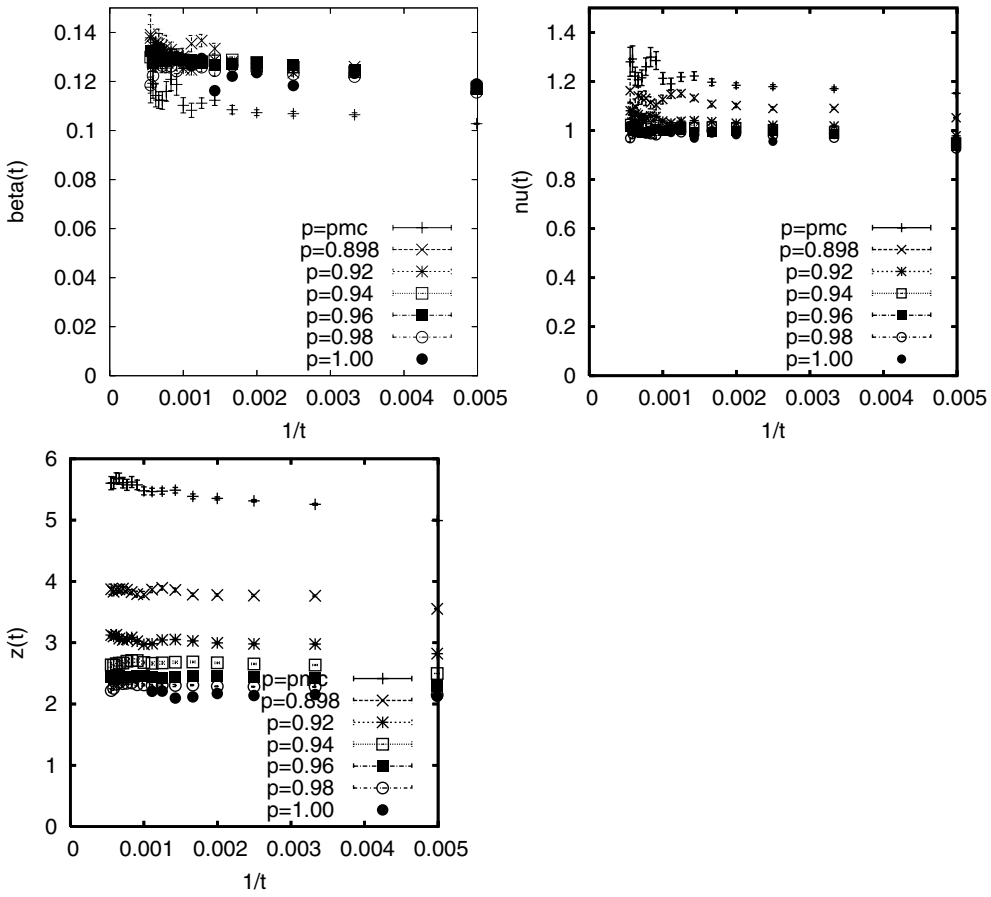

Figure 27. Local exponent $\beta(t)$, $\nu(t)$ and $z(t)$ for the 2D $\pm J$ Ising model [113].

no long range order in continuous spin systems [118], while the KT phase appears in the XY model. In this phase, there is no spontaneous magnetization but the correlation length always diverges. Since the correlation length increases exponentially as T approaches the KT transition temperature T_{KT} from disordered phase, it is difficult to analyse large systems by the EMCS [119–123].

In the KT transition, another difficulty arises in the analysis of EMCS. Let us consider finite size scaling analyses with the domain-wall free energy [124], Roomany-Wyld's beta function [125] or Binder's cumulant [126], which have been standard methods for second-order transitions. These functions change the size dependence and become scale invariant at the critical point. Therefore, data curves for several sizes plotted with respect to the temperature show crossing at the transition point, and one can estimate it. On the other hand, these quantities show scale invariance whole in the KT phase as well as tat the KT transition point, since the correlation length always diverges there. Then, the data curves merge below the transition point, and it becomes difficult to estimate it[5].

[5] Precisely speaking, not all terms in the expansion with respect to the inverse of the scale factor become scale invariant whole in the KT phase, while at least the leading term does so. This provides some misleading in scaling analyses for the KT transitions.

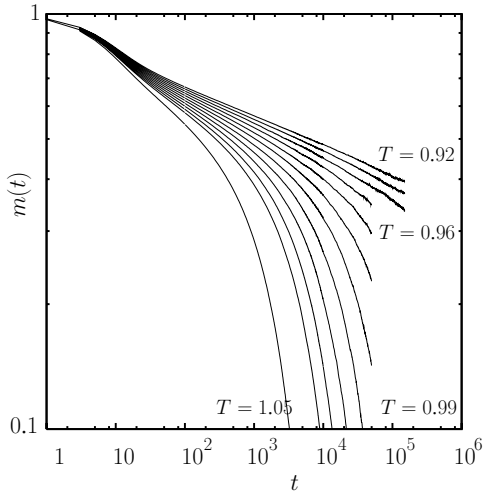

Figure 28. Relaxation of magnetization $m(t)$ for the 2D FM XY model is plotted at $T = 0.92, 0.93, 0.94, 0.95, 0.96, 0.97, 0.98, 0.99, 1.00, 1.01, 1.02, 1.05$ in double-log plot [128].

6.1. Scaling analysis for KT transition temperature

We introduce the NER analysis of the KT transition [127, 128]. A similar analysis has already been attempted [129, 130] in a different manner. The present method is simple and easy to apply to various systems. We propose a scaling analysis to estimate accurate transition point and exponent with a systematic procedure for very large systems.

As an example, let us consider the XY model in two dimensions

$$\mathcal{H} = -J \sum_{\langle ij \rangle} \cos(\theta_i - \theta_j), \tag{6.1}$$

where the variable θ_i takes any values in $[0, 2\pi)$. The transition of the PM and KT phases occurs at $T = T_{\mathrm{KT}}$. We observe the relaxation of magnetization from the all-aligned state as in the analysis of the FM case. The result for $1.05 \geqslant T \geqslant 0.92$ is plotted in figure 28. Calculations are carried out mainly on the 1001×1000 square lattice with the skew boundary condition up to the observation time 1.5×10^5 MCS. About $192 \sim 640$ independent runs are performed for averaging. The size dependence is checked to be negligible, when we compare the data with those for 1501×1500 for some temperatures. For efficiency of calculation, we discretize the spin state and use the 1024-states clock model. This discretization is checked to be negligible, when we compare the data with the 2048-state model.

Similar to the finite-size-scaling analysis in the EMCS, we cannot distinguish the transition point and the KT phase regime from the relaxation behaviour directly, since it is always power law inside the KT phase. This point is much different from the NER analysis for standard second-order transition systems in section 2. Due to the critical relaxation in the KT phase, it is not apparent that the observed power-law behaviour keeps in a longer time regime. In fact, in $0.94 \geqslant T \geqslant 0.92$ in figure 28, which is higher than the expected T_{KT}, the relaxation behaviour keeps almost power law within the observed time $t \leqslant 1.5 \times 10^5$ MCS.

In figure 28, one can see a coherent behaviour of the relaxation function $m(t)$ in the regime of $T > T_{\mathrm{KT}}$. After some initial relaxation time which is about 100 MCS, it decays like in a power law up to a definite time τ. Then, a crossover occurs, and it changes to decay

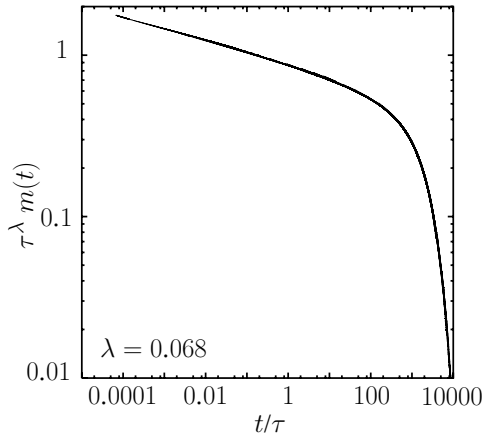

Figure 29. Scaling plot of magnetization curves corresponding to figure 28 is shown [128] for all the temperatures in $1.05 \geqslant T \geqslant 0.92$ to equation (6.2) with appropriately chosen $\tau(\varepsilon)$ (see figure 30) and λ.

exponentially. The time scale τ is called the relaxation time depending on the temperature. Therefore, it is natural to expect the scaling form [127, 128] for the PM phase regime

$$m(t, \varepsilon) = \tau(\varepsilon)^{-\lambda} \bar{m}[t/\tau(\varepsilon)] \qquad \left(\varepsilon \equiv \frac{|T - T_{\mathrm{KT}}|}{T_{\mathrm{KT}}}\right), \tag{6.2}$$

where λ is the dynamic exponent. We use this scaling form to estimate T_{KT} precisely from the NER function. This method is similar to that used in low-dimensional quantum systems [131, 132], in which the correlation function and resulting correlation length are used instead of the relaxation function and the relaxation time.

First, we estimate $\tau(\varepsilon)$ at each temperature using the scaling form (6.2), and plot $\tau^{\lambda} m(t)$ as a function of t/τ in a double-log scale with independent scaling parameters λ and τ. In this fitting, it is somehow easy to decide the best fitting parameters, since changing the parameter τ causes just the parallel translation of curve. Practically, since λ is constant independent of temperature, we first fix λ, and estimate τ at each temperature. It is repeated for several values of λ. The best value of λ is determined by minimizing the total amount of fitting residual. The result with $\lambda = 0.068(6)$ is shown in figure 29. The estimated τ are plotted in figure 30.

Next we determine T_{KT} from the estimated $\tau(\varepsilon)$. As T approaches T_{KT}, the correlation length diverges exponentially [116, 117] as

$$\xi \sim \exp(a'/\sqrt{\varepsilon}). \tag{6.3}$$

We expect that the relaxation time diverges in the same way

$$\tau(\varepsilon) = b \exp(a/\sqrt{\varepsilon}) \tag{6.4}$$

instead of a power-law divergence in standard second-order transitions. It is reasonable if one assumes the relation $\tau \sim \xi^z$ with a definite value of z. Using the χ^2 fitting with parameters a, b and T_{KT}, we obtain the best fitting as shown in figure 30 with $T_{\mathrm{KT}} = 0.894(4)$. The result is consistent with those obtained so far [119–123, 129] especially with the recent ones obtained by the EMCS [122, 123].

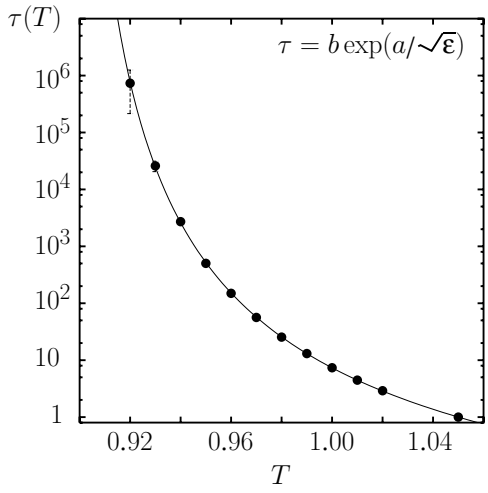

Figure 30. Relaxation times $\tau(\varepsilon)$ corresponding to figures (28) and (29) are plotted [128] in a unit of τ at $T = 1.05$. The curve fitted to equation (6.4) with $T_{\rm KT} = 0.894$ is shown.

6.2. FM–KT transition

It is noted that the scaling relation (6.2) can be applied to the FM–KT transition point as well as the PM–KT one. As an example, let us see the analysis for the six-state clock model [128], which is a discrete-state version of the XY model. In the q-state clock model in two dimensions with $q \geqslant 5$, it is pointed out that there exist successive phase transitions of PM–KT–FM phases [133] at $T = T_{\rm KT1}$ and $T = T_{\rm KT2} < T_{\rm KT1}$.

To analyse both transitions, we calculate the relaxation of magnetization in $1.01 \geqslant T \geqslant 0.60$. The results are plotted in figure 31. For the higher transition point $T = T_{\rm KT1}$, a similar analysis with the continuous case is made for the data in $1.01 \geqslant T \geqslant 0.93$, and gives the result as $\lambda = 0.067(6)$ and $T_{\rm KT1} = 0.899(5)$. For the lower transition point $T = T_{\rm KT2}$, the scaling plot of the data in $0.68 \geqslant T \geqslant 0.60$ fitted to equation (6.2) with $\lambda = 0.029(3)$ is shown in figure 32. Note that the scaling functions $\bar{m}(x)$ in equation (6.2) for higher and lower transition points are different from each other, while the scaling form is the same. The estimated relaxation times are plotted in figure 33. The χ^2 fitting to equation (6.4) is also shown with $T_{\rm KT2} = 0.704(5)$. The result is consistent with those obtained so far [134–136].

6.3. Some applications

The NER analysis for KT transitions has been used successfully to study various problems. Here, we show some example of applications for KT systems including frustration and/or randomness, which reveals a serious slow relaxation.

The first example is the FFXY models in two dimensions [64, 65]. For the FFXY models, as discussed in section 5.1, the possibility of two different transitions, the chiral transition and the KT one, has been discussed. Since the works in [82, 99], there has been another controversy concerning to the transition temperatures, $T_{\rm KT}$ and $T_{\rm c}$, for these transitions, i.e. the double transitions ($T_{\rm KT} < T_{\rm c}$) or the single transition ($T_{\rm KT} = T_{\rm c}$). While many works devoted on this problem, recent studies have supported the double transitions [90–92, 94, 95, 98, 102]. The similar NER calculations have been applied to these models, and the scaling

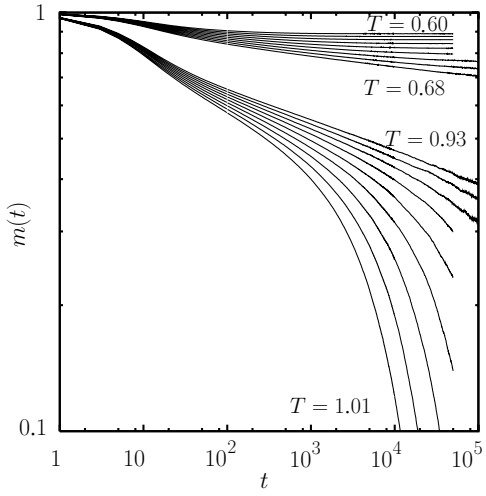

Figure 31. Relaxation of magnetization $m(t)$ for the 2D FM 6-state clock model is shown [128] for $T = 0.60$, 0.61, 0.62, 0.63, 0.64, 0.65, 0.66, 0.67, 0.68, and for 0.93, 0.94, 0.95, 0.96, 0.97, 0.98, 0.99, 1.00, 1.01 in double-log plot.

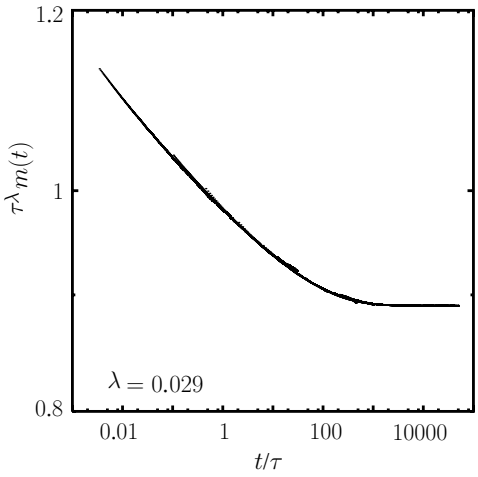

Figure 32. Scaling plot of magnetization curves corresponding to figure 31 is shown [128] for all the temperatures in $0.68 \geqslant T \geqslant 0.60$ to equation (6.2) with appropriately chosen $\tau(\varepsilon)$ (see figure 33) and λ.

analysis provided the KT transition temperature as $T_{\mathrm{KT}} = 0.449(1)$ for the square lattice and $T_{\mathrm{KT}} = 0.508(1)$ for the triangular lattice. As compared with the chiral transition temperatures in table 1, clear deviations were observed between two transition temperatures for both models. This conclude the existence of the double transitions.

The second example is the gauge glass (GG) model in two dimensions [137–139] to show the stability of the KT phase against small disorder. The GG model is a classical spin system with quenched disorder; the Hamiltonian is described by equation (5.1), where A_{ij} is a

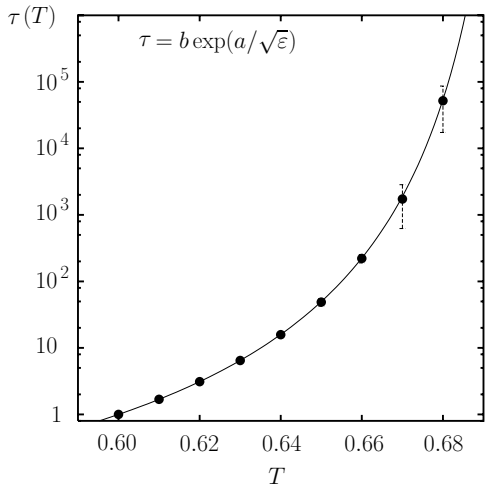

Figure 33. Relaxation times $\tau(\varepsilon)$ corresponding to figures (31) and (32) are plotted [128] in a unit of τ at $T = 0.60$. The curve fitted to equation (6.4) with $T_{\mathrm{KT}} = 0.704$ is shown.

quenched random variable. It describes thermodynamics of various systems such as disordered magnets with random Dzyaloshinskii–Moriya interaction [140], Josephson-junction arrays with positional disorder in a magnetic field [141], and so on. In weakly disordered regime in two dimensions, there has been a controversy about the existence of re-entrant transition from the KT phase to the non-KT one [140–153]. With all these studies, the instability of the KT phase against a small disorder has been pointed out by the perturbation expansion and the RG analysis [154, 155]. However, it is denied by numerical simulations [148, 149, 152, 153] and other RG analyses [147, 149–151]. Analytically, the gauge theory which has provided several exact relations in Ising SG models shows the absence of re-entrance if the KT phase appears in finite disordered regime [156]. The same result is also derived from a dynamical point of view obtained by the dynamical gauge theory [157]. While the results of gauge theory are plausible, the stability of the KT phase is necessary to be assumed. The same NER analysis has applied to locate the MCP for this system, and it has clearly been confirmed the stability of the KT phase against small disorder [137–139].

The analysis has also been applied to the melting transition in the hard-disk system in two dimensions [158–160]. While this system is not frustrated, the simulation for such particle models takes much time and the KT transition with respect to the bond-orientational order reveals the slow relaxation. The NER analysis concluded the existence of the KT transition which is consistent with the Kosterlitz–Thouless–Halperin–Nelson–Young theory [161, 162].

6.4. Estimation of critical exponents

Here, we propose the NER analysis of critical exponents for KT transition systems applying the NER of fluctuations like in section 3. The exponents just at the KT transition point are examined. At the transition point, we assume a power-law relaxation of order parameter $m(t) \sim t^{-\lambda}$. For second-order transition cases, the dynamical exponent λ is relating to conventional ones, equation (2.13), which is derived from the dynamic scaling hypothesis (2.11). However, it cannot be used for the KT transition case, since the magnetization is always vanishing in the equilibrium state.

Instead of that, let us consider the relaxation of a correlation function (2.4) for the spin variable

$$G(r,t) \equiv \langle S_0(t) \cdot S_r(t) \rangle, \tag{6.5}$$

which, in the critical regime, obeys the scaling relation

$$G(r,t) = r^{-\eta} g[t/\tau(r)]. \tag{6.6}$$

The function $\tau(r)$ is the crossover time for the length scale r defined in equation (2.5). For $t \ll \tau(r)$, two spins, S_0 and S_r, behave almost independently, and for $t \gg \tau(r)$, they correlate with each other as in the equilibrium state. In other words, if one obtains $\xi(t)$, the correlation length at time t by solving $\tau(\xi) = t$, two spins behave independently for $r \gg \xi(t)$ and they correlate with each other as in the equilibrium state for $r \ll \xi(t)$. These facts reveal the asymptotic behaviour of G:

$$G(r,t) \sim \begin{cases} r^{-\eta} & (t \gg \tau(r) \quad \text{or} \quad r \ll \xi(t)) \\ m(t)^2 & (t \ll \tau(r) \quad \text{or} \quad r \gg \xi(t)). \end{cases} \tag{6.7}$$

The crossover time $\tau(r)$ is increasing with r up to the bulk relaxation time, or equivalently, the correlation length $\xi(t)$ is spreading with t up to the bulk correlation length. Therefore, we may assume $\tau(r) \sim r^z$ or $\xi(t) \sim t^{1/z}$ at the critical point. Consequently, we obtain the relation

$$\lambda = \frac{\eta}{2z}. \tag{6.8}$$

To estimate the exponents η and z individually, we use a relaxation of fluctuation, i.e. the dynamical susceptibility

$$\chi(t) \equiv \frac{1}{N} \sum_{i,j} \langle S_i(t) S_j(t) \rangle - \left(\sum_i \langle S_i(t) \rangle \right)^2 \tag{6.9}$$

$$= \sum_i (G(r_i,t) - m(t)^2). \tag{6.10}$$

Because of equation (6.7), only the terms in the correlated regime $r_i \leqslant \xi(t)$ are contributed to the summation. If one considers the sufficiently large time so that $m(t)$ is negligible, he/she obtains

$$\chi(t) \sim \int_0^{\xi(t)} r^{-\eta} r \, \mathrm{d}r, \tag{6.11}$$

which is diverging as $t^{\frac{2-\eta}{z}}$. It is convenient to consider the function

$$f_{mm}(t) \equiv N[\langle m^2 \rangle / \langle m \rangle^2 - 1], \tag{6.12}$$

which is algebraically diverging as $t \to \infty$ with the exponent

$$\lambda_{mm} = \frac{2}{z}. \tag{6.13}$$

We have applied this method for six kinds of models [163]: (a) the FM XY model on the square lattice, (b) the FM six-state clock model on the square lattice, (c) the FFXY model on the square lattice, (d) the AFXY model on the triangular lattice, (e) the GG model (cosine type) on the square lattice, and (f) the GG model (Villain type) on the square lattice. For (e) and (f), the transition at the MCP is investigated. The studies on the critical exponents for KT transition systems have not been presented much because of its difficulties in numerical simulations. For the model (a), Kosterlitz [117] derived $\eta = 1/4$ using the RG method. The method was extended to the clock models [133], and derived $\eta = 1/4$ at the upper transition

Table 4. Summary of estimated critical exponents together with critical temperatures used for the calculation [163].

	Model	T_{KT}	η	z
(a)	FM XY model	0.894(4)	0.25(1)	2.10(10)
(b)	FM six-clock model	0.899(5)	0.24(1)	2.05(10)
(c)	FF XY model (square)	0.449(1)	0.305(15)	1.90(5)
(d)	AF XY model (Triangle)	0.508(1)	0.310(15)	1.90(15)
(e)	GG model (cosine)	0.325(6)	0.16(1)	2.10(15)
(f)	GG model (Villain)	0.370(12)	0.13(1)	2.10(15)

point and $1/9$ at the lower one for the model (b). Recent numerical estimations by MC [123], $\eta = 0.243$ and $\eta = 0.113$, are consistent with them. For the model (c), $\eta = 0.22$ was estimated by MC [92], while $\eta = 0.34$ was obtained by using 19-vertex model which would be equivalent to the model (c) [93]. For the exponent z, it was estimated as $z = 2.0$ by MC for the model (a) [164].

The results are summarized in table 4. For regular systems (a) and (b), the estimated values of η are consistent with the RG analyses [117, 133], $\eta = 1/4$. This would support the validity of the present NER analysis for KT systems. The estimations, $\eta \sim 0.31$, for fully frustrated systems (c) and (d), and $\eta \sim 0.15$, for GG models (e) and (f) are clearly deviated from $1/4$. It is remarkable that the exponent η seems to be classified into some classes. Although the results for regular systems are in good agreement with the reliable RG ones, we have no guarantees that the method also gives similar good estimations in more complicated systems, the FF systems, the multi-critical point for the GG systems and so on. As for the dynamic exponent z, the results also indicate a classification, while the values are distributed around $z \sim 2.0$ with small differences. To conclude these pictures, we need further calculations, i.e. analyses for relaxations of a longer time scale.

7. Spin glass transition

The picture of the spin glass (SG) phase is established in the mean-field level [165, 166] based on the replica symmetry breaking (RSB) [167–169]. It is characterized by the multi-valley structure of the free energy landscape in the order parameter space with the so-called ultrametric structure. Since the upper critical dimensions of SG systems are large, such a mean-field picture might be improper in some physical situations. Studies on short-range SG models have played an important role to interpret and understand the experimentally observed SG phenomena. Now the lower critical dimensions of the SG transitions and the validity of the RSB picture in short-range SG models are the important remaining problems. Since randomness and frustration make it difficult to treat short-range SG models analytically as well as numerically, many efforts have been devoted to overcome it in last three decades.

In this section, we examine the applicability of the NER method to SG transitions. Slow dynamics is one of the peculiar properties characterizing the SG phase [169–177]. A typical realization of slow dynamics is the so-called 'aging' [171–175]. The relaxation behaviour depends strongly on the waiting time from which the environment of the system is changed. Since the equilibration time in real SG materials would be longer than the observation time, the SG phenomena observed in experiments are originated in the NER process to the equilibrium state. While direct analysis for an equilibrium state has been a main part of the SG theory to show that the phenomenon is a kind of thermodynamic phase transitions, analysis for

NER is also an important step to understand the SG. Recent progress on the theory of SG is partly owing to studies on nonequilibrium phenomena [173–178]. In the NER analysis of SG systems, the frustration and randomness which restrict possible system sizes in EMCS do not affect directly, and one may simulate much larger systems. Further, since the statistical averaging is taken from independent samples, it is easy to eliminate the systematic errors which are likely to mislead the conclusions of simulation study—the confirmation of the asymptotic relaxation still remains. In spite of such advantages for the NER method, some problems arise for the extension.

If one tries to make an NER analysis as in the second-order transition case in section 2, it is difficult to prepare a good initial, nonequilibrium state, which is the all-aligned one in the FM case. Further, it is difficult to find a good dynamical order parameter instead of the magnetization. These problems correspond to the question of the proper static-order parameter for the equilibrium SG phase. To overcome this difficulty, we show two kinds of analyses. One is the observation of the clone correlation function (CCF) [174–177, 179], which is the relaxation of the replica overlap from a fixed state. The other is based on the evolution of the SG susceptibility [180, 181]. It is similar to the NER of fluctuations in section 3 for the estimation of critical exponents. In both cases, we need to use the scaling hypothesis like the analysis for KT transition systems in section 6, where we loose the advantage of the NER method in the second-order transition case, in which the transition temperature is estimated with a much reliable error bar.

7.1. Relaxation of replica overlap

First, we examine a dynamical quantity $Q(t, t_{\rm w})$ called the clone correlation function (CCF) [127, 182]. It measures the spin correlation between real replicas produced after the relaxation with a waiting time $t_{\rm w}$ from an all-aligned state, which we call the starting state[6]. It is found that the asymptotic behaviour of the CCF and the scaling behaviour around $t = t_{\rm w}$ provide a new dynamical way for the estimation of the SG transition temperature, which is obtained with much larger sizes. It is shown that the asymptotic behaviour of the CCF in the SG phase is quite different from that in the FM phase. This indicates a complex phase space like in the mean-field model [185]. Let us consider a system relaxed in the heat bath for time interval $t_{\rm w}$ from the all-aligned state. It is recognized as a preparation of the initial state ($t = 0$) for relaxation. Then, produce two replicated systems ($S^{(1)}$ and $S^{(2)}$) and simulate them independently. The overlap of these two replicas is calculated

$$Q(t, t_{\rm w}) \equiv \left[\left\langle S_i^{(1)}(t + t_{\rm w}) S_i^{(2)}(t + t_{\rm w})\right\rangle_{t_{\rm w}}^{\rm F}\right]_{\rm c}, \tag{7.1}$$

where $\langle \cdots \rangle_{t_{\rm w}}^{\rm F}$ represents the dynamical average in the above process and $[\cdots]_{\rm c}$ represents the average for disorder. It is equal to unity at $t = 0$. The waiting time $t_{\rm w}$ plays a role to magnify the amplitude of the slowest mode relatively, while the SG order of this initial state is still incomplete.

As an example, we investigate the behaviour of the CCF for the $\pm J$ Ising SG model in three dimensions; the Hamiltonian is shown in equation (5.4). Here, the quenched random variable J_{ij} takes values $+J$ or $-J$ independently with equal weights. In the middle of 1980s, some extensive and efficient Monte Carlo simulations were presented for this model [179, 186, 187]. The equilibrium quantities relevant to SG transitions were estimated to conclude the existence of the SG phase. The estimated transition temperature, $T_{\rm g} = 1.175 \sim 1.2$, was consistent with that obtained by series expansion,[188] providing the confirmation of the equilibrium

[6] The dynamical behaviour is not affected by the fixed starting state in SG systems. It becomes independent after the average for disorder [183, 184, 157].

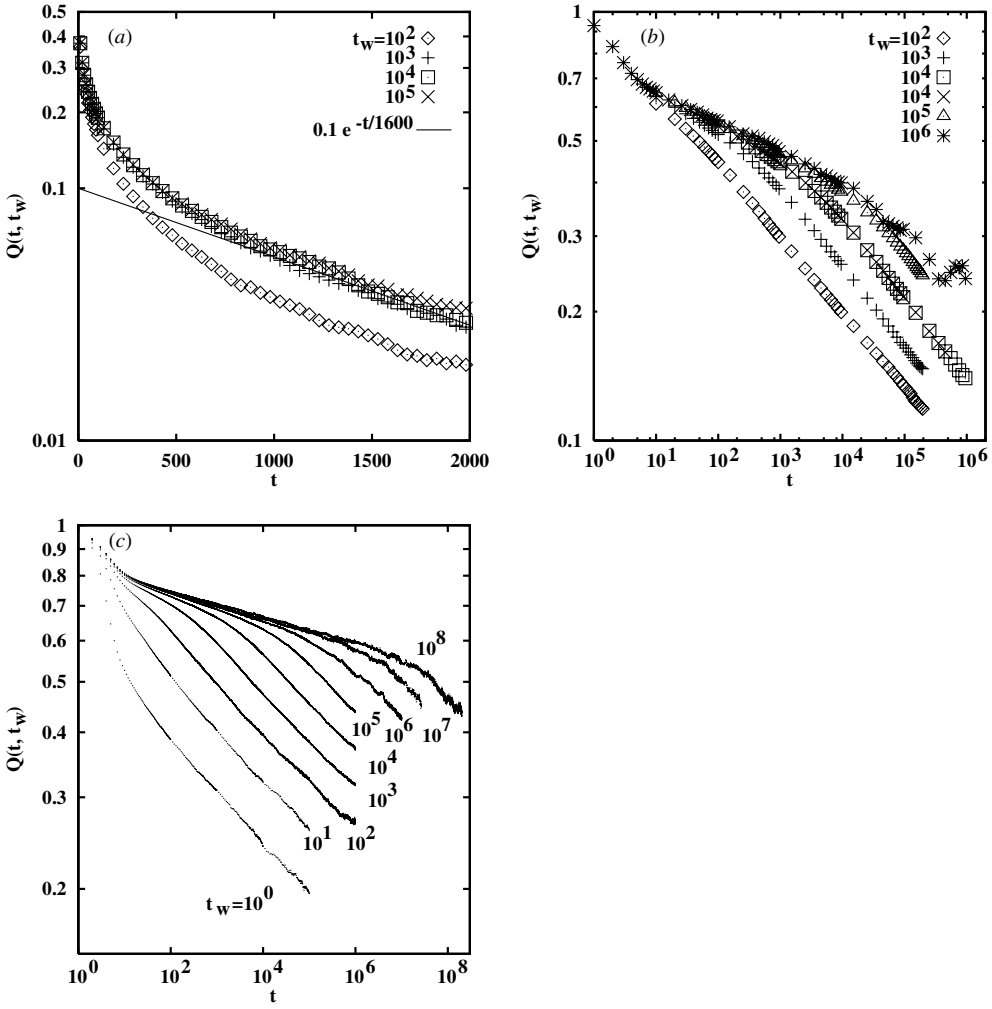

Figure 34. Behaviour of the CCF is shown for the simple-cubic lattice of several temperatures [38], (*a*) $T = 1.6$, (*b*) $T = 1.2$ and (*c*) $T = 0.9$. The solid line in (a) is shown to guide the eyes to give an idea of the relaxation time-scale. Figure (a) is a semi-log plot, and figures (b) and (c) are double-log plots.

SG transition in three dimensions. The recent result obtained by Monte Carlo simulation in equilibrium states [189] with the same strategy as in [179] shows a slightly lower value of the SG transition temperature, $T_g = 1.11(4)$.

Typical behaviour of the CCF are shown in figure 34. Simple-cubic lattices with sizes from $29^2 \times 30$ up to $127^2 \times 128$ were simulated. The simulations are performed for several temperatures with times up to $t_w = 10^8$ and $t = 2 \times 10^8$. The size dependence is checked for several sizes, and it is confirmed that these lattices are large enough to eliminate the finite-size effects up to the present maximum time of simulations within the present accuracy. The number of independent bond configurations N_b is chosen from tens to thousands for each temperature T. In the PM phase (figure 34(*a*), $T = 1.6$), $Q(t, t_w)$ shows an exponential decay in time t. Here, the decay time is called the thermalization time and denoted by τ_{th}. It does

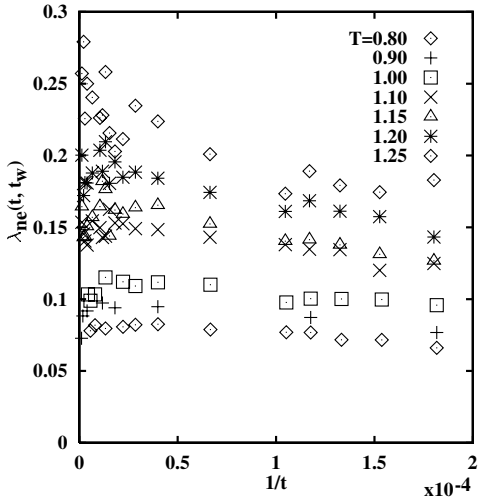

Figure 35. Local exponents $\lambda_q(t, t_w)$ as functions of $1/t$ with $t_w = 10^4$ fixed [182]. The curves bend upwards as $t \to \infty$ for $T \geqslant 1.25$, as expected for the PM phase.

Table 5. The asymptotic behaviour of the CCF for each temperature region. Two time regimes, $t < t_w$ and $t > t_w$, are distinguished.

Temperature	$T < T_g$	$T = T_g$	$T > T_g$
$t < t_w$	Finite order	Power	Exponential
$t > t_w$	Power	Power	Exponential

not depend on the waiting time t_w but on the temperature T for large t_w. It is observed that $Q(t, t_w)$ shows t_w-dependence if $t_w < \tau_{th}$, while it is independent of t_w if $t_w > \tau_{th}$. When $t_w > \tau_{th}$, the starting state relaxes during the waiting time, and the state at $t = 0$ reaches an equilibrium state. $Q(t, t_w)$ shows a replica-overlap relaxation in equilibrium. On the other hand, when $t_w < \tau_{th}$, the initial state is not an equilibrium state and depends on t_w. Therefore, the CCF involves two time scales, τ_{th} and t_w, in the PM phase.

At a temperature close to the critical point (figure 34(*b*), $T = 1.2$) or in the SG phase (figure 34(*c*), $T = 0.9$), $Q(t, t_w)$ shows a power-law decay in time t and the amplitude depends on t_w. The waiting time dependence is clearly observed and it gives the time scale of dynamical behaviour. A crossover is found from one power law to the other at around $t \sim t_w$. In the regime of $t \ll t_w$, $Q(t, t_w)$ does not depend on t_w if t_w is large enough, while it does in the asymptotic regime $t \gg t_w$. The decay exponent for $t \gg t_w$ seems to be independent of t_w. Such a crossover appears in a wide range of temperature below T_g. This is a part of aging phenomena characteristic to SG systems [171–173]. The behaviour of the CCF for each temperature regions is summarized in table 5.

We define the local exponent of $Q(t, t_w)$ as

$$\lambda(t, t_w) \equiv -\frac{\mathrm{d} \log Q(t, t_w)}{\mathrm{d} \log t} \tag{7.2}$$

to analyse the asymptotic behaviour more clearly. Practically, the local exponent $\lambda(t, t_w)$ is estimated by the least square fitting of $\log Q(t, t_w)$ to $\log t$ in a finite time interval. In figure 35, we plot $\lambda(t, t_w)$ for the case of $t_w = 10^4$ MCS. It is clearly observed that the curves for

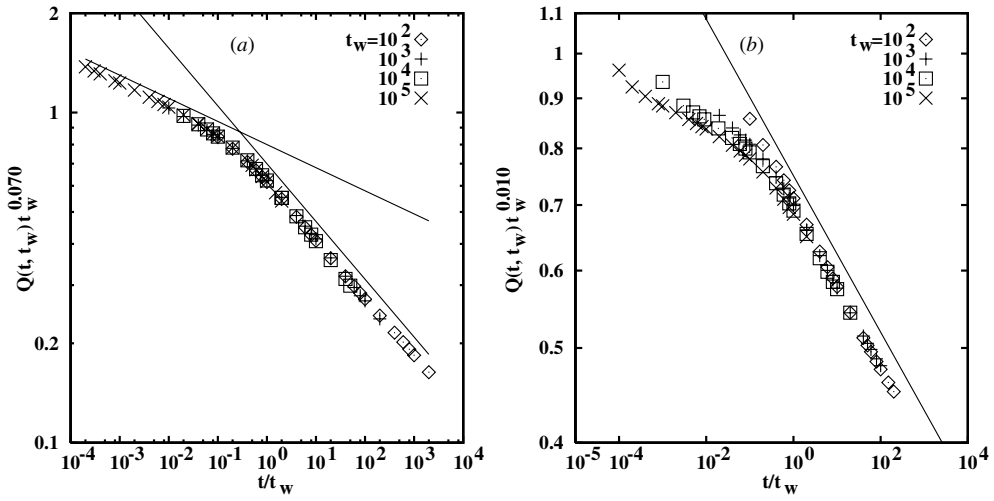

Figure 36. Scaling plot of $Q(t, t_w)$ at (*a*) $T = 1.20$ and (*b*) $T = 0.8$ in three dimensions. Values of scaling exponent are selected so that the points fall onto scaling curve for $t/t_w \gg 1$ [182]. (*a*) At $T = 1.20$ which is close to the transition temperature, not only the region for $t/t_w \gg 1$, but also that for $t/t_w \ll 1$ are scaled by the single exponent. Solid lines show $a \cdot (t/t_w)^{-0.070}$ and $b \cdot (t/t_w)^{-0.175}$. (*b*) At $T = 0.80$, only the region $t/t_w \gg 1$ is scaled. Solid line shows $c \cdot (t/t_w)^{-0.080}$.

$T \geqslant 1.25$ turn up when $1/t$ goes to zero—indicating the PM phase in this temperature region. This is consistent with the expected transition temperature [179, 186–189] $1.11 \leqslant T_g \leqslant 1.2$. Note that the curves for $T \leqslant 1.2$ approach nonzero finite values—indicating a power-law decay of $Q(t, t_w)$. This means that the SG transition temperature is located around $T = 1.2$. The temperature $T = 1.25$ is the upper bound of T_g in this analysis [182].

The above analysis does not give an estimation for the lower bound of T_g, since the downward behaviour which usually means the finite ordering is not observed for the CCF in the SG phase. The following scaling analysis supplements this problem [182]. At the critical temperature, time scales included in $Q(t, t_w)$ are just t and t_w. Thus, one can expect the scaling form

$$Q(t, t_w) = t_w^{-\lambda_q} \bar{q}(t/t_w), \tag{7.3}$$

which is numerically confirmed for $T = 1.2$ in figure 36(*a*) with $\lambda_q = 0.070$. This scaling relation is not observed for $T < T_g$. As an example, in figure 36(*b*), we plot $t_w^{\lambda} \cdot Q(t, t_w)$ for $T = 0.8$ with λ chosen to fit curves in the regime $t/t_w > 1$; the asymptotic power is t_w-independent in this regime. Clearly, curves are spread in $t/t_w < 1$ and the scaling form (7.3) is not satisfied in the whole t/t_w regime. A similar feature is observed also at $T = 1.0$ and 0.9. Therefore, we conclude that the scaling relation (7.3) is valid only in the critical region near the critical point. The result at $T = 1.1$ also shows the scaling form (7.3) both for $t/t_w > 1$ and $t/t_w < 1$. The region $1.1 \leqslant T \leqslant 1.2$ is regarded as the critical region within this simulation. If one estimates the CCF more accurately or for a longer time interval, higher resolution would be available.

7.2. Scaling analysis for dynamical SG susceptibility

As shown in section 3, one can identify the transition point using the NER of fluctuations instead of the order parameter. Another way to estimate the SG transition temperature has

been proposed by Nakamura *et al* [190–192]. They analysed the dynamical SG susceptibility [180, 181] using the scaling hypothesis. In the equilibrium state for the Ising case, the SG susceptibility is defined by

$$\chi_{\mathrm{SG}} = \frac{1}{N}\sum_{i,j}[\langle S_i S_j\rangle^2]_{\mathrm{c}}, \tag{7.4}$$

which is diverging at the SG transition temperature $T = T_{\mathrm{g}}$ as

$$\chi_{\mathrm{SG}} \sim |T - T_{\mathrm{g}}|^{-\gamma}. \tag{7.5}$$

Note that the exponent γ as well as those appearing in this subsection are the SG critical exponents. In the NER analysis, the dynamical SG susceptibility

$$\chi_{\mathrm{SG}}(t) = \frac{1}{N}\sum_{i,j}\left[\langle S_i(t)S_j(t)\rangle_t^2\right]_{\mathrm{c}} \tag{7.6}$$

is measured, where $\langle\cdots\rangle_t$ denotes the dynamical average for the process with a random initial state. Practically, one needs to simulate several numbers of replicated systems simultaneously, i.e. $\left\{S_i^{(\alpha)}\right\}$ $(\alpha = 1, \ldots, m)$ for m replicas. For each pair of replicas, the replica overlap is measured in the simulation; the overlap between two replicas α and β is defined by

$$q^{\alpha\beta}(t) \equiv \frac{1}{N}\sum_i S_i^{(\alpha)}(t)S_i^{(\beta)}(t). \tag{7.7}$$

Then, the SG susceptibility is estimated as

$$\chi_{\mathrm{SG}}(t) = N\left[\frac{2}{m(m-1)}\sum_{\alpha>\beta}\{q^{\alpha\beta}(t)\}^2\right]_{\mathrm{c}}. \tag{7.8}$$

It is noted that the overlap $q^{\alpha\beta}(t)$ is a quantity corresponding to the CCF $Q(t, t_{\mathrm{w}})$ of $t_{\mathrm{w}} = 0$ with a different initial state; the difference of the number of replicas, which is many for the former case and is 2 for the latter case, is not so important after the average for disorder.

Unlikely to the FM case, the asymptotic behaviour of $\chi_{\mathrm{SG}}(t)$ in low-temperature phase has been unclear. Therefore, we use the finite-time scaling hypothesis

$$\chi_{\mathrm{SG}}(t) = \tau(\varepsilon)^{\gamma/z\nu}g(t/\tau(\varepsilon)) \qquad \left(\varepsilon \equiv \frac{|T - T_{\mathrm{g}}|}{T_{\mathrm{g}}}\right) \tag{7.9}$$

for the data above T_{g} as is applied to the KT transition in equation (6.2). In this case, the relaxation time $\tau(\varepsilon)$ is expected to diverge algebraically as

$$\tau(\varepsilon) \sim \varepsilon^{-z\nu} \tag{7.10}$$

instead of the exponential divergence (6.4) for the KT transition. For the $\pm J$ Ising SG model in three dimensions, the analysis was applied with the sizes up to $L = 29$ and the number of replicas up to $m = 9$ [191]; the transition temperature was estimated as $T_{\mathrm{g}} = 1.17(4)$ with the exponents $\gamma/z\nu = 0.3875(75)$, $z\nu = 9.3(12)$ and $\gamma = 3.7(5)$.

The same analysis has been applied to other SG models, i.e. the $\pm JXY$ model and the $\pm J$ Heisenberg model in three dimensions. In such continuous SG models, there has been a controversy about the existence of the SG transition in three dimensions. Numerical studies in 1980s suggested that there is no SG transition [193–196]. Thus the lower critical dimensions had been believed to be 4 or larger. Since the experimentally observed SG materials are well approximated by these continuous models, some explanations have been necessary in the theory. While Kawamura proposed a chirality mechanism to explain it [197–199], recent

simulations including the NER analysis have improved the results and concluded the existence of the SG transition [190, 191, 200, 201].

In continuous spin models, one needs to consider the vector spins, and the definition of the SG susceptibility (7.6) is replaced by

$$\chi_{\mathrm{SG}}(t) = \frac{1}{N}\sum_{i,j}\left[\langle \mathbf{S}_i(t)\cdot\mathbf{S}_j(t)\rangle_t^2\right]_{\mathrm{c}}. \tag{7.11}$$

Then, the replica overlap (7.7) needs to include the indices μ and ν for the spin component x, y (and zt) as

$$q^{\alpha\beta}_{\mu,\nu}(t) \equiv \frac{1}{N}\sum_i S^{(\alpha)}_{i,\mu}(t)S^{(\beta)}_{i,\nu}(t) \tag{7.12}$$

and

$$\chi_{\mathrm{SG}}(t) = N\left[\frac{2}{m(m-1)}\sum_{\alpha>\beta}\sum_{\mu,\nu}\left\{q^{\alpha\beta}_{\mu,\nu}(t)\right\}^2\right]_{\mathrm{c}}. \tag{7.13}$$

For the $\pm J$ Heisenberg SG model in three dimensions, the analysis was applied with the sizes up to $L = 59$ and the number of replicas up to $m = 9$ [191]; the transition temperature was estimated as $T_{\mathrm{g}} = 0.20(2)$ with the exponents $\gamma/z\nu = 0.39(5)$, $z\nu = 4.8(10)$ and $\gamma = 1.9(5)$.

If one needs to consider the chiral glass transition, he/she may estimate the chiral spin $C_{i,\phi}$ instead of the spin variable S_i, which is the scalar chirality for the Heisenberg case, and the z-component of the vector chirality for the XY case.

8. Quantum system

The NER method has also been applied to quantum systems [202, 203]. The quantum Monte Carlo (QMC) simulation based on the Suzuki–Trotter decomposition [15] is used. The d-dimensional quantum system is mapped on to an equivalent $(d+1)$-dimensional classical system. The additional dimension is called the Trotter direction and its length is called the Trotter number denoted by M. The original quantum system is recovered in the limit of the infinite Trotter number. In the studies for phase transitions in finite temperatures, the NER method can be applied directly. One may calculate the relaxation of order parameter for some value(s) of Trotter number, and estimate that in the limit of $M \to \infty$. This estimation is achieved by a standard extrapolation of data with M, or one can use data for a definite value of M in the time interval up to when the data behave independent of M. The independence is checked by comparing the data for several values of M, which is similar to the check of size dependence in the standard NER analysis. Note that the NER calculated in the above QMC is due to the statistical dynamics and not due to the intrinsic one in the quantum mechanics. Even so, it is possible to detect the phase transition, since the critical slowing down must appear in the $(d+1)$-dimensional classical system if the continuous phase transition occurs in the original d-dimensional quantum system.

The method can be extended to the ground state phase transitions in which the quantum fluctuation reveals the transition essentially. In such cases, it is difficult to analyse the system directly by the Monte Carlo simulation, since it cannot work without the thermal fluctuation. To study the ground state by QMC, one may simulate a system with $M/L^{\bar{z}}$ and $Mk_{\mathrm{B}}T$ fixed and estimate the limit of $L \to \infty$. In the NER analysis, the parameter (system size) L can be taken large so as to ignore the finite size effect in the observed time regime. This means, in the quantum case, the simulated system can be regarded as that in the ground state.

The system with a larger Trotter number provides a longer time of critical relaxation, which reveals the true transition point. The critical exponents [202, 203] as well as the transition point [204, 205] can be estimated at the ground state.

While the QMC is effective in many systems, it includes some problems, i.e. the extrapolation for M, and the so-called Wiesler freezing. In the standard QMC, the acceptance rate of the world-line flip becomes worse as the Trotter number increases. This phenomenon is based on a technical problem in the formulation of QMC, not from any physical origin. Recently, a new dynamics has been proposed for QMC to solve these problems, which is called the loop algorithm [9, 10]. Non-local clusters in the $(d+1)$-dimensional space are produced following the Boltzmann weight, and the spins on each cluster are flipped simultaneously, which accelerate the simulation efficiently. In this algorithm, the limit of the infinite Trotter number can be taken beforehand [206].

Nakamura [207] proposed an extension of the loop algorithm to the NER method for quantum systems. In principle, the NER analysis cannot be applied to the cluster dynamics with non-local cluster flip, since the critical relaxation in which the order parameter shows a power-law decay does not appear in it. If one uses the original loop algorithm, the same difficulty occurs. His idea is to produce loops (clusters) in which the connection is global in the Trotter direction while that is local in the real space. To do so, it is necessary to modify the connection rule to produce a cluster. That in the Trotter direction is the same, while, in the real space direction, additional Boltzmann weight is calculated for the flipping rate. Because of the local connection in the real space, the spacial correlation is conducting locally in one Monte Carlo step. Then, one can simulate a system with a much large (infinite) Trotter number, and observe the critical relaxation. The method was applied to the one-dimensional case [207], in which the loop is defined for every two real sites.

9. Remarks

The nonequilibrium relaxation (NER) method is reviewed to analyse equilibrium phase transitions and critical phenomena. It provides the transition point as well as critical exponents. The method can be applied to the second-order phase transition as well as other various transitions. Since 1990s, the method has been applied to quantitative analyses, and now becomes one standard strategy to study the phase transition and critical phenomena. Main advantage of the method originates in the facts that the behaviour in the thermodynamic limit is observed more easily and that equilibration is not necessary. It can be applied to a wide variety of phases and transitions in various statistical models. For example, ferromagnetic (FM) phases [28–30, 34–40, 50–52, 54, 62, 63, 66, 110, 111, 129, 185, 208, 209, 210], antiferromagnetic (AF) phases [211], chiral phases [64, 65, 81, 96, 212], Kosterlitz–Thouless (KT) phases [61, 64, 65, 127, 128, 138, 139, 158–160, 163, 209, 213], spin glass (SG) phases [182, 190–192], partial disordered phases [213], staggered quadrupole phases [60], successive phase transitions [60], first-order phase transitions [61, 68, 76], multi-critical regimes [111], dynamical phase transitions, have been treated. The FM Ising model [28–30, 34–37, 39, 40, 52, 54, 66, 129], the Potts models [50, 51, 68, 76, 129], the clock models [61, 214, 128, 163], the polyhedral models [61] the Baxter model [215], the FM XY model [61, 127, 130, 163, 212], the FM Heisenberg model [61] the antiferromagnetic-next-nearest neighbour Ising (ANNNI) model [213], the layered triangular AF Ising model [216], the fully frustrated XY model [64, 65, 96, 163], the triangular-lattice AF XY models [81, 64, 65, 163], the Blume–Emery–Griffiths model [60, 137], the ϕ^4 field theory [209] the $SU(2)$ lattice gauge theory [217] the two-dimensional hard-disk model [158–160], the random-bond Ising model [210], the $\pm J$ Ising SG model [38, 62, 63, 110, 111, 182, 185, 208], the XY SG model

[191, 192], the Heisenberg SG model [190, 191], the gauge glass model [138, 139, 163, 185], the random field XY model, the one-dimensional contact process [218], the one-dimensional quantum spin chain models [204, 207, 205], the two-dimensional quantum Heisenberg models [202, 203] have been investigated by the NER method.

Acknowledgments

The authors thank S Fukushima, K Hukushima, K Kasono, H Kitatani, G A Kohring, T Matsuhisa, S Miyashita, Y Murase, K Ogawa, H Watanabe and S Yukawa for their collaborations. They also thank K Binder, H J Herrmann, D P Landau, T Nakamura, H Nishimori, Y Nonomura, K Okamoto, D Stauffer, M Suzuki, H Takano, H Takayama and B Zheng for fruitful discussions and comments.

References

[1] Baxter R J 1982 *Exactly Solved Models in Statistical Mechanics* (London: Academic)
[2] Metropolis N, Rosenbluth A W, Rosenbluth M N, Teller A H and Teller E 1953 *J. Chem. Phys.* **21** 1087
[3] Fermi E, Pasta J and Ulam S 1955 Studies of the nonlinear problems: I *Los Alamos Report* LA-1940
[4] Alder B J and Wainwright T E 1957 *J. Chem. Phys.* **27** 1208
[5] Moore G E 1965 *Eloctronics* **38** 9
[6] Barber M N 1983 *Phase Transitions and Critical Phenomena* vol 8 ed C Domb and J L Lebowitz (London: Academic) p 145
[7] Landau D P and Binder K 2005 *A Guide to Monte Carlo Simulations in Statistical Physics* 2nd edn (Cambridge: Cambridge University Press)
[8] Swendsen R H and Wang J S 1987 *Phys. Rev. Lett.* **58** 86
[9] Evertz H G, Lana G and Marcu M 1993 *Phys. Rev. Lett.* **70** 875
[10] Wiese U J and Ying H P 1994 *Z. Phys.* B **93** 147
[11] Berg B A and Neuhaus T 1991 *Phys. Lett.* B **267** 249
[12] Berg B A and Neuhaus T 1992 *Phys. Rev. Lett.* **68** 9
[13] Hukushima K and Nemoto K 1996 *J. Phys. Soc. Japan* **65** 1604
[14] Ito N and Kohring G A 1994 *Int. J. Mod. Phys.* C **5** 1
[15] Suzuki M 1976 *Phys. Lett.* A **58** 435
[16] Suzuki M 1977 *Prog. Theor. Phys.* **58** 1142
[17] Hohenberg P C and Halperin B I 1977 *Rev. Mod. Phys.* **49** 435
[18] Gunton J D, San Miguel M and Sahni P S 1983 *Phase Transitions and Critical Phenomena* vol 8 ed C Domb and J L Lebowitz (London: Academic) p 267
[19] Jan N, Moseley L L and Stauffer D 1983 *J. Stat. Phys.* **33** 1
[20] Sadiq A and Binder K 1984 *J. Stat. Phys.* **35** 517
[21] Kalle C 1984 *J. Phys. A: Math. Gen.* **17** L801
[22] Williams J 1985 *J. Phys. A: Math. Gen.* **18** 1781
[23] Kikuchi M and Okabe Y 1985 *Phys. Rev. Lett.* **55** 1220
[24] Kikuchi M and Okabe Y 1986 *J. Phys. Soc. Japan* **55** 1359
[25] Ito N and Suzuki M 1987 *Prog. Theor. Phys.* **77** 1391
[26] Stauffer D 1992 *Physica* A **186** 197
[27] Kohring G A and Stauffer D 1992 *Int. J. Mod. Phys.* C **3** 1165
[28] Ito N 1993 *Physica* A **192** 604
[29] Ito N 1993 *Physica* A **196** 591
[30] Li Z B, Ritschel U and Zheng B 1994 *J. Phys. A: Math. Gen.* **27** L837
[31] Wang F G and Hu C K 1997 *Phys. Rev.* E **56** 2310
[32] Wang J S 1992 *Computer Simulation Studies in Condensed Matter Physics: XI* ed D P Landau, K K Mon and H B Schüttler (Heiderberg: Springer) p 125
[33] Ito N and Kohring G A 1993 *Physica* A **201** 547
[34] Li Z B, Schülke L and Zheng B 1995 *Phys. Rev. Lett.* **74** 3396
[35] Li Z B, Schülke L and Zheng B 1996 *Phys. Rev.* E **53** 2940
[36] Ito N, Ogawa K, Hukushima K and Ozeki Y 2000 *Prog. Theor. Phys. Suppl.* **138** 555

[37] Ito N, Hukushima K, Ogawa K and Ozeki Y 2000 *J. Phys. Soc. Japan* **69** 1931
[38] Ozeki Y and Ito N 2000 *J. Phys. Soc. Japan* Suppl. A **69** 193
[39] Ito N and Ozeki Y 2001 *Computer Simulation Studies in Condensed Matter Physics: XIII* ed D P Landau, S P Lweis and H B Schüttler (Heiderberg: Springer) p 175
[40] Ito N 2005 *Pramana J. Phys.* 64 871
[41] Salman Z and Adler J 1998 *Int. J. Mod. Phys.* C **9** 195
[42] Ferrenberg A M and Landau D P 1991 *Phys. Rev.* B **44** 5081
[43] Ito N and Suzuki M 1991 *J. Phys. Soc. Japan* **60** 1978
[44] Pawley G S, Swendsen R H, Wallace D J and Wilson K G 1984 *Phys. Rev.* B **29** 4030
[45] Blöte H W J, Compagner A, Croockewit J H, Fonk Y T J C, Heringa J R, Hoogland A, Smit T S and van Willigen A L 1989 *Physica* A **161** 1
[46] Baillie C F, Gupta R, Hawick K A and Pawley G S 1992 *Phys. Rev.* B **45** 10438
[47] Blöte H W J, Luijten E and Heringa J R 1995 *J. Phys. A: Math. Gen.* **28** 6289
[48] Talapov A L and Blöte H W J 1996 *J. Phys. A: Math. Gen.* **29** 5727
[49] Murase Y 2007 *Master Thesis* The University of Tokyo
[50] Schülke L and Zheng B 1995 *Phys. Lett.* A **204** 295
[51] Schülke L and Zheng B 1996 *Phys. Lett.* A **215** 81
[52] Ito N and Ozeki Y 1999 *Int. J. Mod. Phys.* C **10** 1495
[53] Milchev A, Heermann D W and Binder K 1986 *Z. Phys.* B **63** 521
[54] Ito N and Ozeki Y 2001 *APPC 2000, Proc. 8th Asia-Pacific Physics Conference* ed Y D Yao, H Y Cheng, C S Chang and S F Lee (Singapore: World Scientific) p 277
[55] Wansleben S and Landau D P 1991 *Phys. Rev.* B **43** 6006
[56] Stauffer D and Knecht R 1996 *Int. J. Mod. Phys.* C **7** 893
[57] Gropengiesser U 1995 *Physica* A **215** 308
[58] Guida R and Zinn-Justin J 1998 *J. Phys. A: Math. Gen.* **31** 8103
[59] Campostrini M, Pelissetto A, Rossi P and Vicari E 1999 *Phys. Rev.* E **60** 3526
[60] Ogawa K and Ozeki Y 2000 *J. Phys. Soc. Japan* **69** 2808
[61] Ito N, Fukushima S, Watanabe H and Ozeki Y 2002 *Computer Simulation Studies in Condensed Matter Physics: XIV* ed D P Landau, S P Lweis and H B Schüttler (Heiderberg: Springer) p 27
[62] Ito N and Ozeki Y 2003 *Computer Simulation Studies in Condensed Matter Physics: XV* ed D P Landau, S P Lweis and H B Schüttler (Heiderberg: Springer) p 34
[63] Ito N and Ozeki Y 2003 *Physica* A **321** 262
[64] Ozeki Y and Ito N 2003 *Computer Simulation Studies in Condensed Matter Physics: XV* ed D P Landau, S P Lweis and H B Schüttler (Heiderberg: Springer) p 42
[65] Ozeki Y and Ito N 2003 *Phys. Rev.* B **68** 054414
[66] Ozeki Y and Ito N 2003 *J. Phys. A: Math. Gen.* **36** 5175
[67] Rushbrooke G S 1963 *J. Chem. Phys.* **39** 842
[68] Schülke L and Zheng B 2000 *Phys. Rev.* E **62** 7482
[69] Ferrenberg A M and Swendsen R H 1988 *Phys. Rev. Lett.* **61** 2635
[70] Ferrenberg A M and Swendsen R H 1989 *Phys. Rev. Lett.* **63** 1195
[71] Lee J and Kosterlitz J M 1990 *Phys. Rev. Lett.* **65** 137
[72] Lee J, Kosterlitz J M and Granato E 1991 *Phys. Rev.* B **43** 11531
[73] Binder K and Hermann D W 1992 *Monte Carlo Simulation in Statistical Physics* (Berlin: Springer)
[74] Ferrenberg A M, Landau D P and Binder K 1998 *Phys. Rev.* E **58** 3533
[75] Wu F Y 1982 *Rev. Mod. Phys.* **54** 235
[76] Ozeki Y, Kasono K, Ito N and Miyashita S 2003 *Physica* A **321** 271
[77] Rebbi C 1980 *Phys. Rev.* D **21** 3350
[78] Fucito F and Vulpiani A 1982 *Phys. Lett.* A **89** 33
[79] Villain J 1977 *J. Phys. C: Solid State* **10** 4793
[80] Villain J 1977 *J. Phys. (France)* **38** 26
[81] Ito N 1998 *Computer Simulation Studies in Condensed Matter Physics: XI* ed D P Landau, K K Mon and H B Schüttler (Heiderberg: Springer) p 130
[82] Teitel S and Jayaparakash C 1983 *Phys. Rev.* B **27** 598
[83] Choi M Y and Doniach S 1985 *Phys. Rev.* B **31** 4516
[84] Yosefin M and Domany E 1985 *Phys. Rev.* B **32** 1778
[85] Choi M Y and Stroud D 1985 *Phys. Rev.* B **32** 5773
[86] Berge B, Diep H T, Ghazali A and Lallemand P 1986 *Phys. Rev.* B **34** 3177
[87] Grest G S 1989 *Phys. Rev.* B **39** 9267

[88] Thijssen J M and Knops H J F 1990 *Phys. Rev.* B **42** 2438
[89] Granato E and Nightingale M P 1993 *Phys. Rev.* B **48** 7438
[90] Lee J R 1994 *Phys. Rev.* B **49** 3317
[91] Ramirez-Santiago G and José J V 1994 *Phys. Rev.* B **49** 9567
[92] Lee S and Lee K C 1994 *Phys. Rev.* B **49** 15184
[93] Knops Y M M, Niehuis B, Knops H J F and Blöte H W J 1994 *Phys. Rev.* B **50** 1061
[94] Olsson P 1995 *Phys. Rev. Lett.* **75** 2758
[95] Jeon G S, Park S Y and Choi M Y 1997 *Phys. Rev.* B **55** 14088
[96] Luo H J, Schülke L and Zheng B 1998 *Phys. Rev. Lett.* **81** 180
[97] Luo H J, Schülke L and Zheng B 1998 *Phys. Rev.* E **57** 1327
[98] Korshunov S E 2002 *Phys. Rev. Lett.* **88** 167007
[99] Miyashita S and Shiba H 1984 *J. Phys. Soc. Japan* **53** 1145
[100] Lee D H, Joannopoulos J D, Negele J W and Landau D P 1984 *Phys. Rev. Lett.* **52** 433
[101] Van Himbergen J E 1986 *Phys. Rev.* B **33** 7857
[102] Lee S and Lee K C 1998 *Phys. Rev.* B **57** 8472
[103] Nishimori H 1981 *Prog. Theor. Phys.* **66** 1169
[104] Ozeki Y and Nishimori H 1987 *J. Phys. Soc. Japan* **56** 1568
[105] Ozeki Y and Nishimori H 1987 *J. Phys. Soc. Japan* **56** 3265
[106] Singh R R P 1991 *Phys. Rev. Lett.* **67** 899
[107] Kitatani H 1992 *J. Phys. Soc. Japan* **61** 4049
[108] Ito N 1992 *Computational Approaches in Condensed-Matter Physics* ed S Miyashita, M Imada and H Takayama (Berlin: Springer) p 236
[109] Singh R R P and Adler J 1996 *Phys. Rev.* B **54** 364
[110] Ito N, Matsuhisa T and Kitatani H 1998 *J. Phys. Soc. Japan* **67** 1188
[111] Ozeki Y and Ito N 1998 *J. Phys. A: Math. Gen.* **31** 5451
[112] Hukushima K 2000 *J. Phys. Soc. Japan* **69** 631
[113] Ozeki Y and Ito N in prepartion
[114] Berezinskii V L 1971 *Sov. Phys.—JETP* **32** 493
[115] Berezinskii V L 1971 *Sov. Phys.—JETP* **34** 610
[116] Kosterlitz J M and Thouless D J 1973 *J. Phys. C: Solid State* **6** 1181
[117] Kosterlitz J M 1974 *J. Phys. C: Solid State* **7** 1046
[118] Mermin N D 1967 *J. Math. Phys.* **8** 1061
[119] Tobochnik J and Chester G V 1979 *Phys. Rev.* B **20** 3761
[120] Fernández J F, Ferreira M F and Stankiewicz J 1986 *Phys. Rev.* B **34** 292
[121] Gupta R, DeLapp J and Batrouni G 1988 *Phys. Rev. Lett.* **61** 1996
[122] Dukovski I, Machta J and Chayes L V 2002 *Phys. Rev.* E **65** 026702
[123] Tomita Y and Okabe Y 2002 *Phys. Rev.* B **66** 180401
[124] Müller-Hartmann E and Zittartz J 1977 *Z. Phys.* **27** 261
[125] Roomany H H and Wyld H W 1980 *Phys. Rev.* D **21** 3341
[126] Binder K 1981 *Z. Phys.* B **43** 119
[127] Ozeki Y, Ito N and Ogawa K 2000 *Activity Report 1999* (University of Tokyo: Super Computer Center, ISSP) p 37
[128] Ozeki Y, Ogawa K and Ito N 2003 *Phys. Rev.* E **67** 026702
[129] Zheng B 1998 *Int. J. Mod. Phys.* B **12** 1419
[130] Zheng B, Schulz M and Trimper S 1999 *Phys. Rev.* E **59** 1351
[131] Okamoto K and Nomura K 1992 *Phys. Lett.* A **169** 433
[132] Nomura K and Okamoto K 1994 *J. Phys. A: Math. Gen.* **27** 5773
[133] José J V, Kadanoff L P, Kirkpatrick S and Nelson D R 1977 *Phys. Rev.* B **16** 1217
[134] Tobochnik J 1982 *Phys. Rev.* B **26** 6201
[135] Challa M S S and Landau D P 1986 *Phys. Rev.* B **33** 437
[136] Yamagata A and Ono I 1991 *J. Phys. A: Math. Gen.* **24** 265
[137] Ogawa K 2000 *Master Thesis* Tokyo Institute of Technology (in Japanese)
[138] Ozeki Y and Ogawa K 2005 *Phys. Rev.* B **71** 220407
[139] Ozeki Y 2005 *Prog. Theor. Phys. Suppl.* **157** 86
[140] Rubinstein W, Shraiman B and Nelson D R 1983 *Phys. Rev.* B **27** 1800
[141] Granato E and Kosterlitz J M 1986 *Phys. Rev.* B **33** 6533
[142] Forrester M G, Lee H J, Tinkham M and Lobb C J 1988 *Phys. Rev.* B **37** 5966
[143] Chakrabarti A and Dasgupta C 1988 *Phys. Rev.* B **37** 7557

[144] Forrester M G, Benz S P and Lobb C J 1990 *Phys. Rev.* B **41** 8749
[145] Paczuski M and Kardar W 1991 *Phys. Rev.* B **43** 8331
[146] Gingras M J P and Sørensen S 1992 *Phys. Rev.* B **46** 3441
[147] Nattermann T, Scheidl S, Korshunov S E and Li M S 1995 *J. Phys. (France)* I **5** 565
[148] Cha M C and Fertig H A 1995 *Phys. Rev. Lett.* **74** 4867
[149] Jeon S J, Kim S and Choi M Y 1995 *Phys. Rev.* B **51** 16211
[150] Tang L H 1996 *Phys. Rev.* B **54** 3350
[151] Scheidl S 1997 *Phys. Rev.* B **55** 457
[152] Kosterlitz J M and Simkin M V 1997 *Phys. Rev. Lett.* **79** 1098
[153] Maucourt J and Grempel D R 1997 *Phys. Rev.* B **56** 2572
[154] Korshunov S E 1993 *Phys. Rev.* B **48** 1124
[155] Mudry C and Wen X G 1999 *Nucl. Phys.* B **549** 613
[156] Ozeki Y and Nishimori H 1993 *J. Phys. A: Math. Gen.* **26** 3399
[157] Ozeki Y 2003 *J. Phys. A: Math. Gen.* **36** 2673
[158] Watanabe H, Yukawa S, Ozeki Y and Ito N 2002 *Phys. Rev.* E **66** 041110
[159] Watanabe H, Yukawa S, Ozeki Y and Ito N 2004 *Computer Simulation Studies in Condensed Matter Physics XVI* ed D P Landau, S P Lweis and H B Schüttler (Heiderberg: Springer) p 101
[160] Watanabe H, Yukawa S, Ozeki Y and Ito N 2004 *Phys. Rev.* E **69** 045103
[161] Halperin B I and Nelson D R 1978 *Phys. Rev. Lett.* **41** 121
[162] Young A P 1979 *Phys. Rev.* B **19** 1855
[163] Ozeki Y and Ito N 2004 *Computer Simulation Studies in Condensed Matter Physics: XVI* ed D P Landau, S P Lweis and H B Schüttler (Heiderberg: Springer) p 106
[164] Jensen L M, Kim B J and Minnhagen P 2000 *Phys. Rev.* B **61** 15412
[165] Edwards S F and Anderson P W 1975 *J. Phys. F: Metal* **5** 965
[166] Sherrington D and Kirkpatrick S 1975 *Phys. Rev. Lett.* **35** 1972
[167] Binder K and Young A P 1986 *Rev. Mod. Phys.* **58** 801
[168] Mézard M, Parisi G and Virasoro A 1987 *Spin Glass Theory and Beyond* (Singapore: World Scientific)
[169] Fischer K H and Hertz J A 1991 *Spin Glasses* (Cambridge: Cambridge University Press)
[170] Takayama H 1995 *Computational Physics as a New Frontier in Condensed Matter Research* (Japan: Physical Society of Japan) p 230
[171] Lundgren L, Svedlindh P, Nordblad P and Beckman O 1983 *Phys. Rev. Lett.* **51** 911
[172] Vincent E, Hammann J and Ocio M 1992 *Recent Progress in Random Magnets* ed D H Ryan (Singapre: World Scientific) p 207
[173] Rieger H 1993 *J. Phys. A: Math. Gen.* **26** L615
[174] Cugliandolo L F and Dean D S 1995 *J. Phys. A: Math. Gen.* **28** 4213
[175] Barrat A, Burioni R and Mézard M 1996 *J. Phys. A: Math. Gen.* **29** 1311
[176] Takayama H, Yoshino H and Hukushima K 1997 *J. Phys. A: Math. Gen.* **30** 3891
[177] Baldassarri A 1998 *Phys. Rev.* E **58** 7047
[178] Marinari E, Parisi G and Zuliani F 1998 *J. Phys. A: Math. Gen.* **31** 1181
[179] Bhatt R N and Young A P 1985 *Phys. Rev. Lett.* **54** 924
[180] Huse D A 1989 *Phys. Rev.* B **40** 304
[181] Blundell R E, Humayun K and Bray A J 1992 *J. Phys. A: Math. Gen.* **25** L733
[182] Ozeki Y and Ito N 2001 *Phys. Rev.* B **64** 024416
[183] Ozeki Y 1995 *J. Phys. A: Math. Gen.* **28** 3645
[184] Ozeki Y 1997 *J. Phys.: Condens. Matter* **10** 11171
[185] Ozeki Y, Ito N and Ogawa K 2001 *J. Phys. Soc. Japan* **70** 3471
[186] Ogielski A T and Morgenstern I 1985 *Phys. Rev. Lett.* **54** 928
[187] Ogielski A T 1985 *Phys. Rev.* B **32** 7384
[188] Singh R R P and Chakravarty S 1986 *Phys. Rev. Lett.* **57** 245
[189] Kawashima N and Young A P 1996 *Phys. Rev.* B **53** 485(R)
[190] Nakamura T and Endoh S 2002 *J. Phys. Soc. Japan* **71** 2113
[191] Nakamura T, Endoh S and Yamamoto T 2003 *J. Phys. A: Math. Gen.* **36** 10895
[192] Yamamoto T, Sugashima T and Nakamura T 2004 *Phys. Rev.* B **70** 184417
[193] McMillan W L 1985 *Phys. Rev.* B **31** 342
[194] Olive J A, Young A P and Sherrington D 1986 *Phys. Rev.* B **34** 6341
[195] Morris B M, Colborne S G, Moore M A, Bray A J and Canisius J 1986 *J. Phys. C: Solid State* **19** 1157
[196] Jain S and Young A P 1986 *J. Phys. C: Solid State* **19** 3913
[197] Kawamura H and Tanemura M 1991 *J. Phys. Soc. Japan* **60** 608

[198] Kawamura H 1995 *Phys. Rev.* B **51** 12398
[199] Hukushima K and Kawamura H 2000 *Phys. Rev.* E **61** 1008(R)
[200] Maucourt J and Grempel D R 1998 *Phys. Rev.* B **58** 2654
[201] Akino N and Kosterlitz J M 2002 *Phys. Rev.* B **66** 054536
[202] Nonomura Y 1998 *J. Phys. Soc. Japan* **67** 5
[203] Nonomura Y 1998 *J. Phys. A: Math. Gen.* **31** 7939
[204] Nakamura T 2003 *J. Phys. Soc. Japan* **72** 789
[205] Nakamura T 2005 *Phys. Rev.* B **71** 144401
[206] Beard B B and Wiese U J 1996 *Phys. Rev. Lett.* **77** 5130
[207] Nakamura T and Ito Y 2003 *J. Phys. Soc. Japan* **72** 2405
[208] Ito N, Ozeki Y and Kitatani H 1999 *J. Phys. Soc. Japan* **68** 803
[209] Zheng B, Schulz M and Trimper S 1999 *Phys. Rev. Lett.* **82** 1891
[210] Luo H J, Schülke L and Zheng B 2001 *Phys. Rev.* E **64** 036123
[211] Zheng B and Luo H J 2001 *Phys. Rev.* E **63** 066130
[212] Ying H P, Zheng B, Yu Y and Timper S 2001 *Phys. Rev.* E **63** 035101
[213] Shirahata T and Nakamura T 2002 *Phys. Rev.* B **65** 024402
[214] Todoroki N, Ueno Y and Miyashita S 2002 *Phys. Rev.* B **66** 214405
[215] Takano H 1996 *J. Phys. Soc. Japan* **65** 736
[216] Shirahata T and Nakamura T 2004 *J. Phys. Soc. Japan* **73** 254
[217] Okano K, Schülke L and Zheng B 1998 *Phys. Rev.* D **57** 1411
[218] Dickman R 1999 *Phys. Rev.* E **60** R2441